

**COMPUTATIONAL STUDY OF THERMAL ENERGY  
STORAGE SYSTEM BASED ON NANOPARTICLE  
ENHANCED PHASE CHANGE MATERIAL**

**IMAN MOAZEDI**

**RESEARCH PROJECT SUBMITTED IN PARTIAL  
FULFILMENT OF THE REQUIREMENTS FOR THE  
DEGREE OF MASTER OF ENGINEERING**

**FACULTY OF ENGINEERING  
UNIVERSITY OF MALAYA  
KUALA LUMPUR**

**2013**

**UNIVERSITY OF MALAYA**

**ORIGINAL LITERARY WORK DECLARATION**

Registration/Matric No: **KGH100014**

Name of Candidate: **IMAN MOAZEDI**

Name of Degree: **MASTER OF MECHANICAL ENGINEERING**

Title of Project Paper/Research Report/Dissertation/Thesis (“this Work”):

**COMPUTATIONAL STUDY OF THERMAL ENERGY STORAGE SYSTEM  
BASED ON NANOPARTICLE ENHANCED PHASE CHANGE MATERIAL**

Field of Study: **COMPUTATIONAL FLUID DYNAMICS**

I do solemnly and sincerely declare that:

- 1) I am the sole author/writer of this Work;
- 2) This Work is original;
- 3) Any use of any work in which copyright exists was done by way of fair dealing and for permitted purposes and any excerpt or extract from, or reference to or reproduction of any copyright work has been disclosed expressly and sufficiently and the title of the Work and its authorship have been acknowledged in this Work;
- 4) I do not have any actual knowledge nor do I ought reasonably to know that the making of this work constitutes an infringement of any copyright work;
- 5) I hereby assign all and every rights in the copyright to this Work to the University of Malaya (“UM”), who henceforth shall be owner of the copyright in this Work and that any reproduction or use in any form or by any means whatsoever is prohibited without the written consent of UM having been first had and obtained;
- 6) I am fully aware that if in the course of making this Work I have infringed any copyright whether intentionally or otherwise, I may be subject to legal action or any other action as may be determined by UM.

Candidate’s Signature

Date

Subscribed and solemnly declared before,

Witness’s Signature

Date

Name:

Designation:

## **Abstract**

A colloidal mixture of nano-sized particles in a base fluid, called nanofluids, tremendously enhances the heat transfer characteristics of the base fluid, and is ideally suited for practical applications due to its marvelous characteristics. This research report addresses the unique features of nanofluids, such as enhancement of heat transfer, improvement in thermal conductivity, increase in surface volume ratio, Brownian motion, thermophoresis, etc. Improved functionality of phase change materials (PCM) through dispersion of nano particles is reported with preceding application of newly considered geometries as a trapezoidal shape. The resulting nanoparticle-enhanced phase change materials (NEPCM) exhibit enhanced thermal conductivity in comparison to the base material. Starting with steady state natural convection within a differentially-heated trapezoidal cavity that contains a nanofluid (water plus copper nanoparticles), the nanofluid is allowed to undergo solidification. Partly due to increase of thermal conductivity and also lowering of the latent heat of fusion, higher heat release rate of the NEPCM in relation to the conventional PCM is observed. The predicted increase of the heat release rate of the NEPCM is a clear indicator of its great potential for diverse thermal energy storage applications. The investigation of angle variation in a trapezoidal geometry revealed significant enhancement in the solidification of NEPCM. With these improvements, building developers can implement thermal storage systems instead of conventional square cavities without changing the overall area of them.

## **Abstrak**

Satu campuran koloid zarah bersaiz nano dalam bendalir asas, yang dipanggil nanofluids, dengan ketara meningkatkan ciri-ciri pemindahan haba cecair yang asal, dan sangat sesuai untuk aplikasi praktikal kerana ciri-ciri yang menakjubkan. Ini laporan penyelidikan menangani ciri-ciri unik nanofluids, seperti peningkatan pemindahan haba, peningkatan kekonduksian terma, peningkatan dalam nisbah jumlah permukaan, pergerakan Brownian, thermophoresis, dan lain-lain fungsi yang lebih baik daripada bahan-bahan perubahan fasa (PCM) melalui penyebaran zarah nano adalah dilaporkan sebelum permohonan yang baru dianggap geometri sebagai bentuk trapezoid. Terhasil nanoparticle ditambah bahan-bahan perubahan fasa (NEPCM) mempamerkan keberaliran haba dipertingkatkan berbanding dengan bahan asas. Bermula dengan keadaan mantap perolakan semulajadi dalam rongga trapezoid dengan tidak pemanas yang mengandungi nanofluid (air ditambah nanopartikel tembaga), nanofluid itu dibenarkan untuk menjalani pemejalan. Sebahagiannya disebabkan oleh peningkatan kekonduksian haba dan juga menurunkan haba pendam pelakuran, kadar pembebasan haba lebih tinggi NEPCM berhubung dengan PCM konvensional diperhatikan. Ramalan peningkatan kadar pembebasan haba NEPCM adalah petunjuk jelas yang berpotensi besar untuk pelbagai terma aplikasi penyimpanan tenaga. Siasatan variasi sudut dalam geometri trapezoid mendedahkan peningkatan ketara dalam pemejalan NEPCM. Dengan peningkatan ini, pemaju bangunan boleh melaksanakan sistem penyimpanan haba dan bukannya rongga persegi konvensional tanpa mengubah kawasan keseluruhan mereka.

## **Acknowledgements**

I would like to express my deep and sincere gratitude to my supervisor, Sr. Lecturer. Dr. Poo Balan Ganesan for his technical advices and constructive comments throughout this work.

I also would like to appreciate my friend, Mr. Ravi, for all his efforts and helpful recommendations during the completion of this research project.

I want to thank my family for their patience and encouragement, not only for my research work, but in all dimensions of my life.

## Table of Contents

Abstract .....	iii
Abstrak .....	iv
Acknowledgements.....	v
Table of Contents.....	vi
List of Figures.....	ix
List of Tables.....	xi
Nomenclature .....	xii
Chapter 1: Introduction .....	1
1.1 Background .....	1
1.2 Objectives.....	5
1.3 Structure of the Research Project .....	5
Chapter 2: Literature Review .....	6
2.1 Thermal Energy Storage (TES) .....	6
2.2 Phase Change Materials (PCM) .....	10
2.2.1 Classification and Properties .....	11
2.2.1.1 PCM Selection Criteria .....	11
2.2.2 Melting.....	12
2.2.3 Solidification .....	12
2.2.4 Encapsulation of Phase Change Materials .....	12
2.3 Nanofluids .....	13
2.3.1 Type and Application of Nanofluids .....	14
2.3.2 Natural Convection of Nanofluids and Heat Transfer Solution Approaches .....	16

2.3.2.1 Single-Phase Model.....	19
2.3.2.2 Two-Phase Model.....	19
2.3.3 Enhancement of thermal conductivity .....	19
2.3.3.1 Dispersion of the suspended particles.....	20
2.3.3.2 Intensification of turbulence .....	21
2.3.3.3 Brownian motion .....	21
2.3.3.4 Thermophoresis .....	21
2.3.3.5 Diffusiophoresis .....	22
2.3.4 Computational Fluid Dynamics (CFD) .....	23
2.3.5 Finite Volume Method Principles .....	24
2.3.5.1 Advantages and Disadvantages .....	27
Chapter 3: Methodology .....	29
3.1 Boundary Conditions .....	30
3.2 Governing Equations .....	30
3.3 Computational Solution Methods .....	32
3.3.1 Discretization of the Momentum Equation.....	33
3.3.1.1 Pressure Interpolation Schemes.....	33
3.3.2 Discretization of the Continuity Equation .....	35
3.3.2.1 Density Interpolation Schemes.....	36
3.3.3 Pressure-Velocity Coupling .....	37
3.3.3.1 SIMPLE Solution Algorithm .....	37
3.3.3.2 Under-Relaxation .....	39
Chapter 4: Results and Discussions .....	41
4.1 Model Benchmarking.....	41
4.2 Numerically Solved Problem .....	43
4.2.1 Volume Fraction of Solid Particles of $\phi = 0\%$ (Base fluid).....	46

4.2.2 Volume Fraction of Solid Particles of $\phi = 10\%$ (Nanofluid 1) .....	48
4.2.3 Volume Fraction of Solid Particles of $\phi = 20\%$ (Nanofluid 2) .....	48
Chapter 5: Conclusions .....	53
References .....	54

## List of Figures

Figure 1.1 Storage capacity and discharge feature of various forms of energy storage units .....	2
Figure 1.2 Typical groups of materials used as PCM and their latent heats versus melting temperatures .....	3
Figure 2.1 Classification of energy storage materials (Abhat, 1983) .....	10
Figure 2.2 Different geometries for encapsulation of PCM (a) spherical (b) tubular (c) cylindrical and (d) rectangular. ....	13
Figure 2.3 A typical 2D generalized control volume (Jana, Ray, & Durst, 2007) .....	24
Figure 2.4 Numerical treatment of control volumes adjacent to interface and its movement (Jana, et al., 2007) .....	25
Figure 2.5 Movement of typical 2D generalized control volume using cell centered approach (Jana, et al., 2007) .....	25
Figure 3.1 Schematic for the physical model (Khanafar, et al., 2003) .....	29
Figure 3.2 Flow chart showing the SIMPLE Algorithm (Ambatipudi, 2006) .....	39
Figure 4.1 Comparison of the predicted horizontal velocity component on the vertical mid-plane of the square cavity for the present study and those of Khanafar et al. (2003) with $Gr=10^4$ .....	42
Figure 4.2 Comparison of the predicted horizontal velocity component on the vertical mid-plane of the square cavity for the present study and those of Khanafar et al. (2003) with $Gr=10^5$ .....	42
Figure 4.3 Geometry of numerically solved problem.....	43
Figure 4.4 Generated mesh for the shape 1 and shape 2 models of trapezoidal cavity ..	45
Figure 4.5 Colorized contours of the volume fraction of the nanofluid with $\phi = 0\%$ ....	47

Figure 4.6 Colorized contours of the volume fraction of the nanofluid with $\phi = 10\%$ ..	49
Figure 4.7 Colorized contours of the volume fraction of the nanofluid with $\phi = 20\%$ ..	50
Figure 4.8 Liquid fraction-time comparison graph for Shape 1 .....	52
Figure 4.9 Liquid fraction-time comparison graph for Shape 2 .....	52

## List of Tables

Table 4.1 Thermophysical properties of the copper nanoparticles, water ( $\phi=0$ ) and nanofluids with solid copper nanoparticle volume fractions ( $\phi$ ) equal to 0.1 and 0.2 (Khodadadi & Hosseinizadeh, 2007) .....	44
--	----



## **Chapter 1: Introduction**

### **1.1 Background**

Greater energy demand that is faced by any developed or developing economies, uncertainties associated with stable accessibility/supply and pricing of fossil fuels and growing awareness of environmental issues have all contributed to a serious re-examination of various renewable sources of energy. At the same time, the unpredictability of the output of renewable energy conversion systems demands robust, reliable and efficient storage units that are integrated into such systems.

The capacity of storage units used for various forms of energy and the associated depth of discharge (DOD) are shown in Figure 1.1. Among various forms of energy, thermal energy is widely encountered in nature as solar radiation, geothermal energy and thermally stratified layers in oceans. Rejected thermal energy (waste heat) is also a by-product of almost all of the man-made energy conversion systems, equipment and devices. Despite its abundance, thermal energy is generally classified as a low-grade form of energy and is associated with waste in industrial processes. Storage of thermal energy may simply serve as a buffer before it can be used properly or a means of waste heat recovery, providing thermal comfort in buildings, conserving of energy in various sectors of the economy, increasing the operational life of electronics and raising the efficiency of industrial processes.

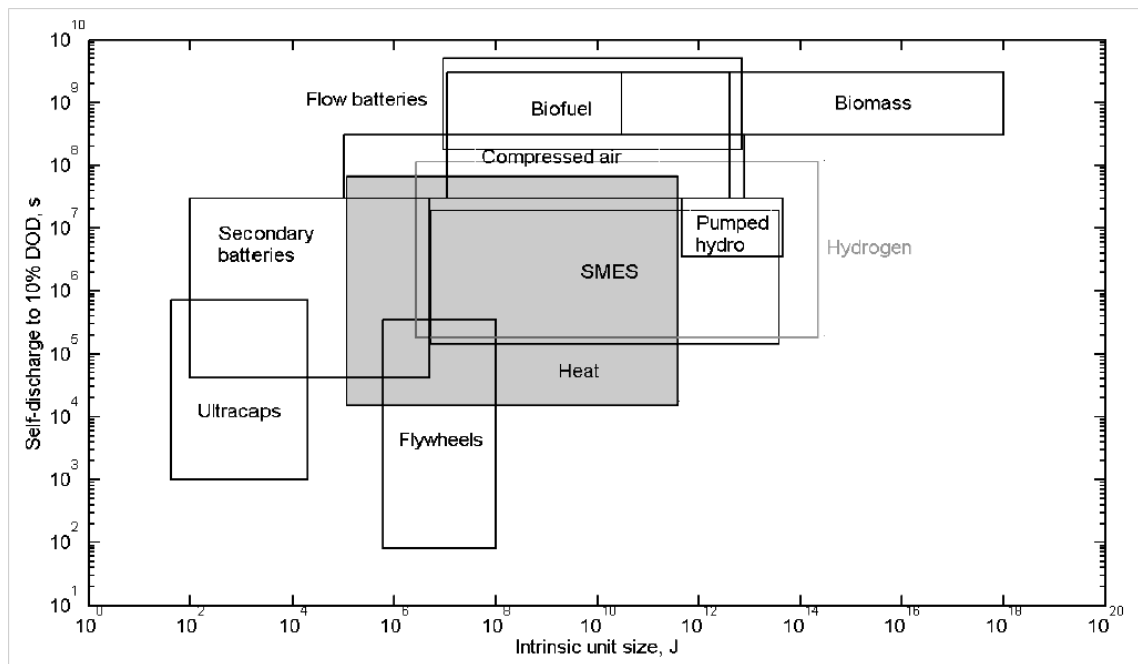


**Figure 1.1 Storage capacity and discharge feature of various forms of energy storage units**

Thermal energy can be stored as sensible or latent heat by heating, melting/evaporating a bulk material. This energy then becomes available when the reverse process is applied. Phase change materials (PCM) are widely used to store/liberate thermal energy by taking advantage of their latent heat (heat of fusion) upon melting/freezing over a narrow temperature range. Storage of thermal energy using PCM has found applications in the areas of thermal management/control of electronics, space power, waste heat recovery and solar thermal utilization for several decades. Early work on thermal energy storage using PCM can directly be linked to thermal control issues related to the fast-paced developments of aeronautics and electronics in the middle of the twentieth century that was followed by the Space Program. The melting/freezing temperature varies over a wide range for different PCM, e.g., paraffins, fatty acids, sugar alcohols, salt hydrates, etc. The latent heat of fusion and the associated phase transformation temperatures of some typical PCM are presented in Figure 1.2. The candidate PCM for a specific application is usually selected with regard to the melting/freezing temperature along with other issues, such as latent heat of fusion, chemical stability, and cost, etc.

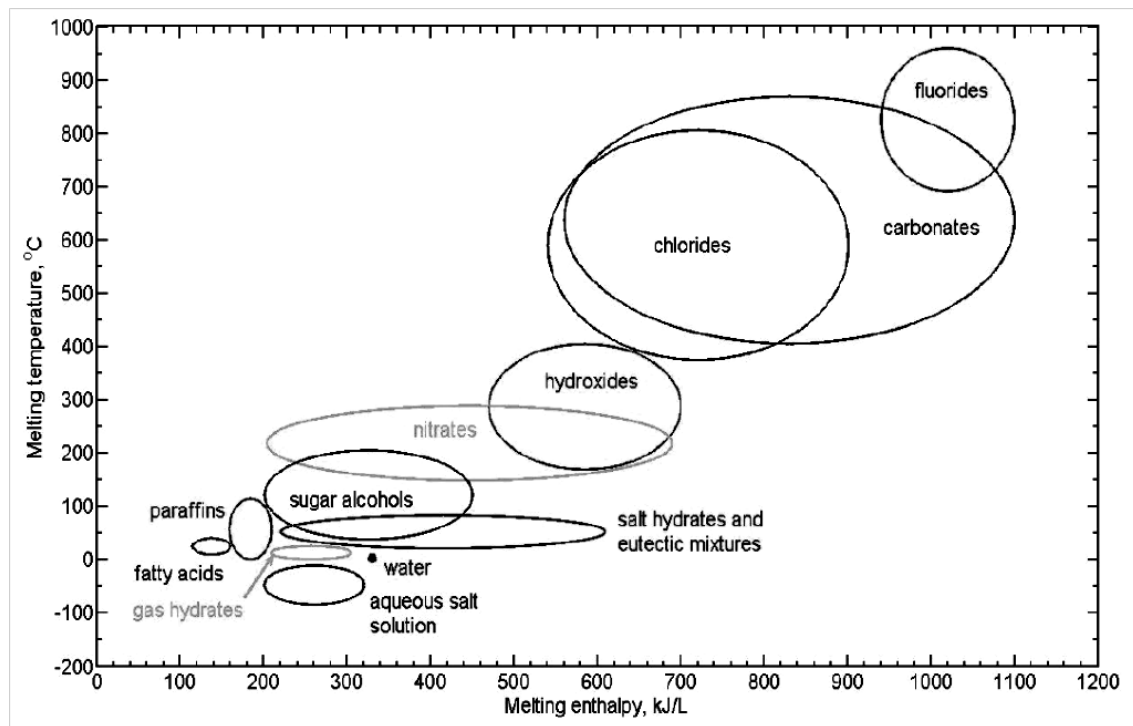


**Figure 1.2 Typical groups of materials used as PCM and their latent heats versus melting temperatures**

A number of review articles discussed candidate PCM, their thermophysical properties, encapsulation, heat transfer enhancement and system-related issues.

An undesirable property of PCM is their relatively low thermal conductivity that strongly suppresses the energy charging/discharging rates. Naturally, forming a composite of the PCM with a thermal conductivity promoter is a logical solution to this problem. Metallic fins and foams and carbon/graphite fibers have been the most favored thermal conductivity promoters, as summarized in a recent overview of the state-of-the-art by Fan and Khodadadi (2011). Literature devoted to thermal conductivity enhancement of PCM-based thermal energy storage systems through utilization of these fixed structures goes back many decades. Determining proper configurations of these fixed enhancers and their interactions with conduction, convection and solid-liquid phase change heat transport mechanisms pose challenging issues.

Other than the fixed structures, the use of highly-conductive powders/beads/particles that are of micron to meso length scale as free-form thermal conductivity enhancers has

also been practiced. Promoted by the rapid development of nanotechnology over the past decades, ultrafine nano-sized particles, which usually possess a nominal diameter of the order of 10 nm, i.e., sub-micron, have become commercially available for various metals and metal oxides. These highly-conductive nanoparticles have been utilized to develop advanced heat transfer fluids, i.e., nanofluids, with considerably enhanced thermal conductivity compared to the base liquids (Yu, France, Routbort, & Choi, 2008). However, the utilization of nanofluids has mainly focused on single-phase and liquid-vapor (boiling) heat transfer applications (Das, Choi, Yu, & Pradeep, 2007), in order to address the increasing challenge associated with thermal management of electronics.

Further utility of this emerging class of liquids as superior and novel PCM, referred to as nano-enhanced PCM (NEPCM), for improved thermal energy storage was recently proposed by Khodadadi and Hosseinizadeh (2007). Due to increase of thermal conductivity, despite lowering of the latent heat of fusion, higher heat release rate of the NEPCM relative to the base PCM was afforded. Comparing to PCM enhanced by fixed fillers and regular-sized particles/beads, the NEPCM colloids will offer better fluidity and smaller contact conductance, and be easier to recycle as well. Since 2007, the great potential of this promising new class of PCM has been increasingly realized. In addition to the efforts devoted to preparation and thermal characterization of PCM with various nanoparticles, experimental investigations on freezing/melting heat transfer of NEPCM have also been conducted, in order to test the performance and to justify the applicability of NEPCM in real-world applications. In addition, the nano-structured additives are not limited to metal and metal oxide nanoparticles and the use of carbon nanofibers and nanotubes, which possess extremely high thermal conductivity, has also been reported (Fan & Khodadadi, 2011).

## **1.2 Objectives**

The objective of this work is to study the effect of various pertinent parameters on the heat transfer within the nanofluid. The detailed objectives of this work are as follows:

- To study the effect of nanoparticle volume fraction on the total solidification time of nanofluid inside the cavity.
- To study the effect of inclination angle of the vertical wall on the total solidification time of nanofluid inside the cavity.

## **1.3 Structure of the Research Project**

The remainder of the present research project consists of five chapters. A comprehensive literature survey on thermal conductivity enhancement of PCM through introduction of thermal storage systems, nanofluids and nano-sized materials will be presented in Chapter 2, followed by a detailed presentation of governing equations and computational methods of solving nanofluids enhanced systems in Chapter 3. A simulated computational analysis directed at exhibiting the expedited freezing of NEPCM will be presented in Chapter 4, in which both volume fractions of solid particles ( $\phi$ ) and angle variations of a trapezoidal shape cavity are applied in an effort to solve the presented numerical example. Finally, concluding remarks will be presented in Chapter 5.

## **Chapter 2: Literature Review**

### **2.1 Thermal Energy Storage (TES)**

Thermal energy storage (TES) in general, and phase change materials in particular, have been a main topic in research for the last 20 years, but although the information is quantitatively enormous, it is also spread widely in the literature, and difficult to find. TES provides solutions in very specific areas (Zalba, Marín, Cabeza, & Mehling, 2003):

- The time delay and available power between production or availability of energy and its consumption in receiving systems (solar energy, cogeneration, etc.)
- Security of energy supply (hospitals, computer centers, etc.)
- Thermal inertia and thermal protection

In the first case, applications related with the use of renewable energies are common, in particular the use of solar energy among others, although applications are also found in cogeneration equipment or in installations with reduced prices for electrical energy consumed during off-peak hours. Nowadays, security of energy supply is often achieved with extra equipment (Zalba, et al., 2003).

The use of phase change materials (PCMs) could either avoid or reduce this extra equipment. As it will be seen later in this research project, thermal inertia and thermal protection is the area where the PCMs have achieved a higher penetration in the market.

Energy demands in the commercial, industrial, utility, and residential sectors vary on a daily, weekly, and seasonal basis. The use of TES in such varied sectors requires that the various TES systems operate synergistically and that they be carefully matched to each specific application. The use of TES for such thermal applications as space heating,

hot water heating, cooling, air-conditioning, and so on has recently received much attention. A variety of new TES techniques has been developed over the past four or five decades in industrial countries (Dincer & Rosen, 2011).

TES systems have enormous potential for making the use of thermal equipment more effective and for facilitating large-scale substitutions of energy resources economically. In general, a coordinated set of actions is needed in several sectors of the energy system for the maximum potential benefits of thermal and other types of energy storage to be realized.

Sensible heat changes in a material are dependent on its specific heat capacity and the temperature change. Latent heat changes are the heat interactions associated with a phase change of a material and occur at a constant temperature. Sensible heat storage systems commonly use rocks or water as the storage medium. Latent heat storage systems can utilize a variety of phase change materials, and usually store heat as the material changes from a solid to a liquid phase (Dincer & Rosen, 2011).

The basic principle is the same in all TES applications. Energy is supplied to a storage system for removal and use at a later time. What mainly varies is the scale of the storage and the storage method used (Dincer & Rosen, 2011). Seasonal storage requires immense storage capacity. One seasonal TES method involves storing heat in underground aquifers. Another suggested method is circulating warmed air into underground caverns packed with solids to store sensible heat (Demirbas, 2006). The domestic version of this concept is storing heat in hot rocks in a cellar. At the opposite end of the storage-duration spectrum is the storage of heat on an hourly or daily basis. The previously mentioned use of tiles to store solar radiation is a typical example which is often applied in passive solar design (Dincer & Rosen, 2011).

Although TES is used in a wide variety of applications, all are designed to operate on a cyclical basis (usually daily, occasionally, and seasonally). The systems achieve benefits by fulfilling one or more of the following purposes (Dincer & Rosen, 2011):

- Increase generation capacity. Demand for heating, cooling, or power is seldom constant over time, and the excess generation available during low-demand periods can be used to charge a TES in order to increase the effective generation capacity during high-demand periods (Velraj, Seeniraj, Hafner, Faber, & Schwarzer, 1999). This process allows a smaller production unit to be installed (or to add capacity without purchasing additional units), and results in a higher load factor for the units.
- Enable better operation of cogeneration plants. Combined heat and power, or cogeneration, plants are generally operated to meet the demands of the connected thermal load, which often results in excess electrical generation during periods of low electricity use (Jegadheeswaran & Pohekar, 2009). By incorporating TES, the plant need not be operated to follow a load. Rather, it can be dispatched in more advantageous ways (within some constraints).
- Shift energy purchases to low-cost periods. This measure constitutes the demand-side application of the first purpose listed, and allows energy consumers subject to time-of-day pricing to shift energy purchases from high- to low-cost periods (Guo & Zhang, 2008).

Effective utilization of time-dependent energy resources requires appropriate TES methods to reduce the time and rate mismatch between energy supply and demand. TES provides a high degree of flexibility since it can be integrated with a variety of energy technologies, for example, solar collectors, biofuel combustors, heat pumps, and off-peak electricity generators (Demirbas, 2006). The heat transfer which occurs when a substance changes from one phase to another is called the latent heat. The latent heat

change is usually much higher than the sensible heat change for a given medium, which is related to its specific heat. When water turns to steam, the latent heat change is of the order of 2MJ/kg.

Most practical systems using phase-change energy storage involve solutions of salts in water. Several problems are associated with such systems, which includes the following (Dincer & Rosen, 2011):

- Super-cooling of the PCM may take place, rather than crystallization with heat release. This problem can be avoided partially by adding small crystals as nucleating agents.
- It is difficult to build a heat exchanger capable of dealing with the agglomeration of varying sizes of crystals that float in the liquid.

The system operation cannot be completely reversed. Any latent heat TES system must possess at least the following three components (Abhat, 1983):

- A heat storage substance that undergoes a phase transition within the desired operating temperature range, and wherein the bulk of the heat added is stored as latent heat.
- Containment for the storage substance.
- A heat-exchange surface for transferring heat from the heat source to the storage substance and from the latter to the heat sink, for example, from a solar collector to the latent TES substance to the load loop.

Some systems use either  $\text{Na}_2\text{SO}_4 \cdot 10 \cdot \text{H}_2\text{O}$  or  $\text{CaCl}_2 \cdot 6\text{H}_2\text{O}$  crystals as their storage media, and employ a heat-exchange oil. The oil is pumped in at the bottom of the storage and rises in globules through the fluid without mixing. Other promising latent TES reactions are those of inter-crystalline changes. Many of these take place at relatively high

temperatures. Solar energy applications require large TES capacities in order to cover a minimum of 1–2 days of thermal demand. This capacity is commonly achieved by sensible heat storage in large water tanks (Jegadheeswaran & Pohekar, 2009). An alternative is offered by latent heat storage systems, where thermal energy is stored as latent heat in substances undergoing a phase transition, for example, the heat of fusion in the solid–liquid transition. The main advantages of latent TES systems are high TES capacities per unit mass compared to those of sensible heat systems, and a small temperature range of operation since the heat interaction occurs at constant temperature. There is no gradual decline in temperature as heat is removed from the PCM (Dincer & Rosen, 2011).

## 2.2 Phase Change Materials (PCM)

In 1983 (Abhat) gave a useful classification of the substances used for TES, shown in Figure 2.1. Among the most thorough references related with phase change materials, one can cite Abhat (1983), Lane (1983, 1986) and Dincer and Rosen (2011).

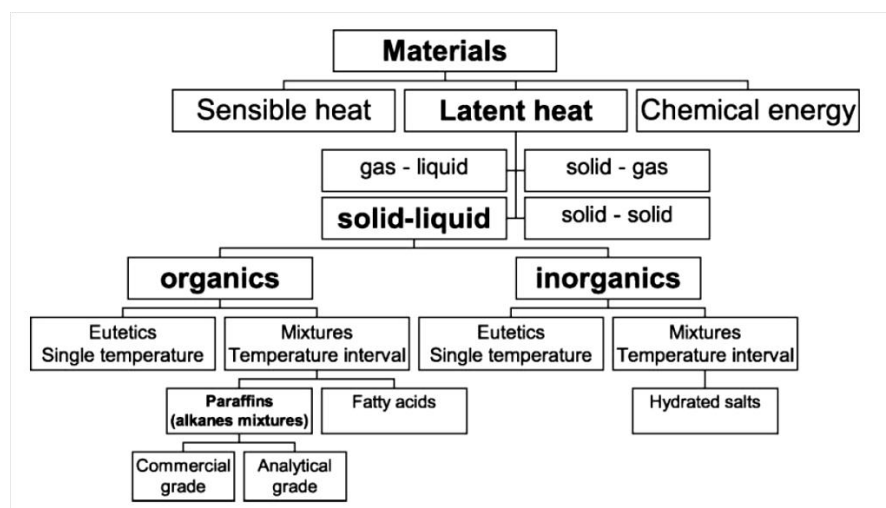


**Figure 2.1 Classification of energy storage materials (Abhat, 1983)**

These contain a complete review of the types of material which have been used, their classification, characteristics, advantages and disadvantages and the various

experimental techniques used to determine the behavior of these materials in melting and solidification.

## **2.2.1 Classification and Properties**

### *2.2.1.1 PCM Selection Criteria*

First of all, it is essential to select the appropriate geometry of the PCM encapsulation. At this point, it is necessary to consider the features that are provided to the storage systems. Power necessity and required operation time are two of these factors. The macro-encapsulation in plate shape has been selected because it is a deeply studied geometry that supposes (Ranjbar, Kashani, Hosseinizadeh, & Ghanbarpour, 2011):

- Facility for controlling the thickness of the PCM, which is a crucial design factor to be able to regulate the time of loading and unloading processes.
- Uniformity of the thickness of the PCM and, therefore, of the phase change process.
- Facility for manufacturing, as much as on small scale as on a large scale, and versatility of handling.
- Commercial accessibility to a wide variety of plate-shape encapsulations of different materials (HDPE, aluminum). Eventually, the aluminum encapsulation is chosen in order to avoid plastic compatibility troubles (Lázaro, Zalba, Bobi, Castellón, & Cabeza, 2006).

Another outstanding factor in order to establish the PCM itself is the temperature range of the application. Depending on the destination room different temperatures are required.

### **2.2.2 Melting**

During melting, heat is transferred to the PCM first by conduction and later by natural convection. This is because, the solid region moves away from the heat transfer surface and the thickness of the liquid region increases near the heat transfer surface. Since thermal conductivity of liquid PCM is less than that of solid PCM, the heat transfer by conduction almost becomes negligible as the melting process continues. The further melting is mostly by natural convection due to the density gradient that exists within the liquid PCM (Jegadheeswaran & Pohekar, 2009).

### **2.2.3 Solidification**

Contrary to melting process, solidification is dominated by conduction. During solidification natural convection exists only in the beginning and as the time goes the effect of natural convection becomes almost zero as compared to the effect of conduction. The heat transfer characteristics of PCM during solidification have been explained by many investigators (Jegadheeswaran & Pohekar, 2009).

### **2.2.4 Encapsulation of Phase Change Materials**

Successful utilization of a PCM requires a means of containment. For active solar systems with a liquid heat-transfer medium, tanks with coil-type heat exchangers are appropriate. For passive or air-cooled active solar systems, much effort has centered on the packaging of a mass of PCM in a sealed container, which itself serves as the heat exchange surface (Dincer & Rosen, 2011).

Potential containers include steel cans, plastic bottles, polyethylene, and polypropylene bottles, high-density polyethylene pipe, flexible plastic film packages, and plastic tubes. The choice of the construction material for the container of a PCM is important. Appropriate tests that are realistic and representative of usage conditions are needed in

any product development (Zalba, et al., 2003). The container material should be an effective barrier that prevents loss of material or water or, when the PCM is hygroscopic, gain water. Oxygen penetration and subsequent oxidization may also be detrimental. The encapsulating material should also be a good heat conductor, so that it facilitates effective heat transfer, and be mechanically resistant to damage from handling, processing, and transport. Systems based on salt hydrates may sometimes have encapsulation problems, particularly in early designs, because of corrosion and fatigue for metals, or water loss through plastics (Dincer & Rosen, 2011).

Macroencapsulation, macro (above 1mm), is a common way of encapsulating the PCM for thermal energy storage applications. The container shape may be spherical, tubular, cylindrical or rectangular as shown in Figure 2.2 (Salunkhe & Shembekar, 2012).

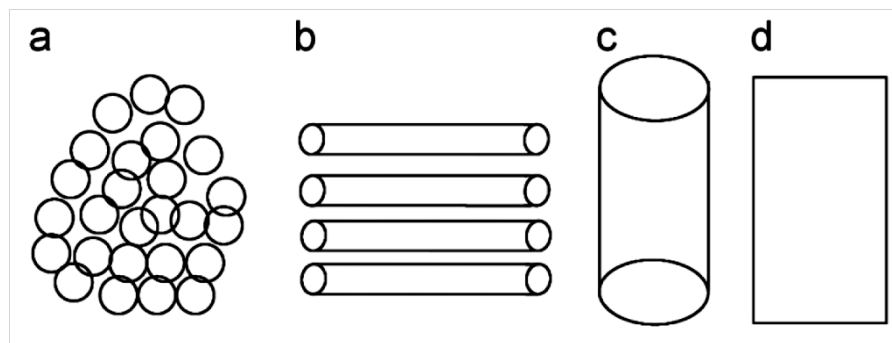


**Figure 2.2 Different geometries for encapsulation of PCM (a) spherical (b) tubular (c) cylindrical and (d) rectangular.**

### 2.3 Nanofluids

Heat transfer fluids such as water, minerals oil and ethylene glycol play an important role in many industrial sectors including power generation, chemical production, air-conditioning, transportation and microelectronics. The performance of these conventional heat transfer fluids is often limited by their low thermal conductivities. According to industrial needs of process intensification and device miniaturization, development of high performance heat transfer fluids has been a subject of numerous

investigations in the past few decades (Wong & De Leon, 2010). It is well known that at room temperature, metallic solids possess an order-of-magnitude higher thermal conductivity than fluids. For example, the thermal conductivity of copper at room temperature is about 700 times greater than that of water and about 3000 times greater than that of engine oil. Therefore, the thermal conductivities of fluids containing suspended solid metallic or nonmetallic (Metallic oxide) particles would be expected to be significantly higher than those of conventional heat transfer fluids (Wu, Zhu, Li, Li, & Lei, 2009).

An inventive way of improving the heat transfer performance of common fluids is to suspend various types of small solid particles, such as metallic, nonmetallic and polymeric particles, in conventional fluids to form colloidal. However, suspended particles of the order of  $\mu\text{m}$  (micrometer) or even mm (millimeter) may cause some problems in the flow channels, increasing pressure drop, causing the particles to quickly settle out of suspension. In recent years, modern nanotechnology has been discovered. Particles of nanometer dimensions dispersed in base liquids are called nanofluids. This term was first introduced by (Choi, 1995). Compared with millimeter or micrometer sized particle suspensions, nanofluids have shown a number of potential advantages such as better long-term stability and rheological properties, and can have significantly higher thermal conductivities.

### **2.3.1 Type and Application of Nanofluids**

Some nanoparticle materials that have been used in nanofluids are oxide ceramics ( $\text{Al}_2\text{O}_3$ , CuO,  $\text{Cu}_2\text{O}$ ), nitride ceramics (AlN, SiN), carbide ceramics (SiC, TiC), metals (Ag, Au, Cu, Fe), semiconductors ( $\text{TiO}_2$ ), single, double or multi-walled carbon (SWCNT, DWCNT, MWCNT), and composite materials such as nanoparticle core-polymer shell composites. In addition new materials and structures are attractive for use

in nanofluids where the particle-liquid interface is doped with various molecules. The base fluids which are used in nanofluids are common heat transfer fluids such as water, engine oil, Ethylene glycol and ethanol (Godson, Raja, Mohan Lal, & Wongwises, 2010).

When the nanoparticles are properly dispersed, nanofluids can offer numerous benefits besides the anomalously high effective thermal conductivity. These properties include (Manca, Jaluria, & Poulikakos, 2010):

*Improved heat transfer and stability:* Because heat transfer takes place at the surface of the particles, it is desirable to use particles with larger surface area. The relatively larger surface areas of nanoparticles compared to microparticles, provide significantly improvement in heat transfer capabilities. In addition, particles finer than 20 nm carry 20% of their atoms on their surface, making them immediately available for thermal interaction. With such ultra-fine particles, nanofluids can flow smoothly in the tiniest of channels such as mini- or microchannels. Because the nanoparticles are small, gravity becomes less important and thus chances of sedimentation are also less, making nanofluids more stable.

*Microchannel cooling without clogging:* Nanofluids will not only be a better medium for heat transfer in general, but they will also be ideal for microchannel applications where high heat loads are encountered. The combination of microchannels and nanofluids will provide both highly conducting fluids and a large heat transfer area. This cannot be attained with macro- or micro-particles because they clog microchannels.

*Miniaturized systems:* Nanofluid technology will support the current industrial trend toward component and system miniaturization by enabling the design of smaller and lighter heat exchanger systems. Miniaturized systems will reduce the inventory of heat transfer fluid and will result in cost savings.

*Reduction in pumping power:* To increase the heat transfer of conventional fluids by a factor of two, the pumping power must usually be increased by a factor of 10. It was shown that by multiplying the thermal conductivity by a factor of three, the heat transfer in the same apparatus was doubled. The required increase in the pumping power will be very moderate unless there is a sharp increase in fluid viscosity. Thus, very large savings in pumping power can be achieved if a large thermal conductivity increase can be achieved with a small volume fraction of nanoparticles. The better stability of nanofluids will prevent rapid settling and reduce clogging in the walls of heat transfer devices. The high thermal conductivity of nanofluids translates into higher energy efficiency, better performance, and lower operating costs. They can reduce energy consumption for pumping heat transfer fluids. Miniaturized systems require smaller inventories of fluids where nanofluids can be used. Thermal systems can be smaller and lighter. In vehicles, smaller components result in better gasoline mileage, fuel savings, lower emissions and a cleaner environment.

### **2.3.2 Natural Convection of Nanofluids and Heat Transfer Solution Approaches**

The natural convection of fluid small-particles suspensions has been used in many applications in the chemical industry, food industry and also in solar collectors (Okada, Kang, Oyama, & Yano, 2001). Comparatively, the natural convection of suspensions is different from that of pure fluids. The natural convection of a suspension is driven by the unstable density distribution of liquid due to temperature differences and the distribution of the particle concentration due to the sedimentation (Kang, Okada, Hattori, & Oyama, 2001). A few studies have reported the natural convection of nanofluids with no, or very little, sedimentation.

Putra et al. (2003) presented the experimental observations on the natural convection of two oxide ( $\text{Al}_2\text{O}_3$  and  $\text{CuO}$ )–water based nanofluids inside a horizontal cylinder heated

from one end and cooled from the other. The dependence of parameters such as particle concentration, particle material and geometry of the containing cylinder were investigated at steady-state conditions. Different from the natural convection of common suspensions, the nature of convection of nanofluids was free from particle concentration gradients and the stratification concentration layers absent. At the same aspect ratio (length to diameter), the natural convective heat transfer of nanofluids was lower than that of the base fluid. However, the natural convective heat transfer of nanofluids deteriorated with increasing particle concentration, aspect ratio of cylinder, and particle density. Even when the particle size of CuO was smaller than that of Al<sub>2</sub>O<sub>3</sub>, the deterioration in heat transfer was greater. This is because the particle density of CuO is higher than Al<sub>2</sub>O<sub>3</sub>.

Due to the absence of experimental data on the natural convection of nanofluids, Khanafer et al. (2003) developed an analytical model to determine the natural convective heat transfer of nanofluids. The nanofluid in the enclosure was assumed to be in single phase, that is both the fluid and particles are in thermal equilibrium and flow at the same velocity. The effect of suspended nanoparticles on the buoyancy-driven heat transfer process was analyzed. It was illustrated that the heat transfer rate increased as the particle volume fraction increased at any given Grashof number.

Kim et al. (2004) proposed an analytical investigation to describe the natural convective heat transfer of nanofluids by introducing a new factor which included the effect of the ratio of thermal conductivity of nanoparticles to that of the base fluid, the shape factor of the particles, the volume fraction of nanoparticles, the ratio of density of nanoparticles to that of the base fluid and the ratio of heat capacity based on the volume of nanoparticles to that of the base fluid. The results showed that the heat transfer coefficients of nanofluid increased with increasing particle volume fraction. With respect to the particle volume fraction, as the heat capacity and density of nanoparticles

increased and the shape factor and the thermal conductivity decreased, the convective motion set in easily (Kim, et al., 2004). However, it is unclear why the results from the analytical approach of Kim and Khanafer were contrary to the experimental results of Putra, the reasons possibly being dependent on the assumptions of the models.

The addition of particles into heat transfer media has been known for a long time as one of the passive techniques for enhancing heat transfer. Compared with the heat transfer enhancement techniques by using suspended millimeter- or micrometer-sized particles, the use of suspended nanoparticles have been more attractive. This is because nanoparticles are ultra-fine and usually used at low particle concentrations. Therefore, they are free from sedimentation that may clog the flow channel. They are also expected to cause little or no penalty in pressure drop. Before applying nanofluids in practical applications, studies on heat transfer and flow characteristics are needed.

Xuan and Roetzel (2000) derived some correlations for predicting the convective heat transfer of nanofluids using two approaches. The first approach treated the nanofluids as a single phase fluid and the other as a solid–liquid mixture. The derived correlations explained that the mechanism of heat transfer enhancement of nanofluids depended on the increasing thermal conductivity of the suspension and the chaotic movement of particles that accelerate the energy exchange process in the fluid. However, there is still a lack of experimental investigation to validate this model.

Afterwards, Xuan and Li (2000) presented an experimental investigation on the convective heat transfer and flow feature of nanofluids. In their experiments, a Cu–water nanofluid was used with the particle concentrations varying between 0.3 and 2% volume fraction and the flows being turbulent in a straight tube. The results indicated that the suspended nanoparticles enhanced the heat transfer of the base fluid, and the convective heat transfer coefficients of the nanofluids increased with increasing flow

velocity and particle concentration. The greater heat transfer enhancement was found to be more than 39% at 2% particle volume fraction. Furthermore, nanofluids caused no significant improvement in pressure drop. There are two different approaches to investigate the enhanced heat transfer of the suspensions: the two-phase one and the single-phase one (Xuan & Li, 2000).

#### *2.3.2.1 Single-Phase Model*

The single phase model provides the possibility of understanding the functions of both the fluid phase and the solid particle in the heat transfer process, but needs much computation time and computer capacity (Xuan & Li, 2000).

#### *2.3.2.2 Two-Phase Model*

By combining Lagrangian statistics and direct numerical simulation, Sato et al. (1998) applied single phase model to analyze the mechanism of two-phase heat and turbulent transport by solid particles (on the micrometer order) suspended in a gas flow, by assuming that the particle enthalpy does not affect the temperature field. The two phase model assumes that both the fluid phase and particles are in a thermal equilibrium state and they flow at the same velocity. This approach is simpler and takes less computation time. In cases that the main interest is focused on heat transfer process, this approach may be more suitable (Xuan & Li, 2000).

### **2.3.3 Enhancement of thermal conductivity**

A substantial increase in liquid thermal conductivity, liquid viscosity, and heat transfer coefficient, are the unique features of nanofluids. It is well known that at room temperature, metals in solid phase have higher thermal conductivities than those of fluids (Kreith, Manglik, & Bohn, 2010). For example, the thermal conductivity of

copper at room temperature is about 700 times greater than that of water and about 3000 times greater than that of engine oil. The thermal conductivity of metallic liquids is much greater than that of nonmetallic liquids. Thus, fluids containing suspended metal particles are expected to manifest enhanced thermal conductivities relative to pure fluids. Masuda et al. (1993) dispersed oxide nanoparticles ( $\gamma$ -Al<sub>2</sub>O<sub>3</sub> and TiO<sub>2</sub> with  $\phi = 4.3\%$ ) particles in liquid and showed the increase in the thermal conductivity to be 32 and 11%, respectively. Eastmann et al. (2001) showed that Cu–ethylene glycol (nanoparticles coated with thioglycolic acid) with  $\phi = 0.3\%$  gave a 40% increase in thermal conductivity. Recently, an attempt at the Indira Gandhi Centre for Atomic Research (IGCAR) was made, to align magnetic nanoparticles (Fe<sub>3</sub>O<sub>4</sub> coated with Oleic acid) in a base fluid (hexadecane) in a linear chain using a magnetic field, which was applied to increase the thermal conductivity by 300% (Philip, Laskar, & Raj, 2008). Further, it was proved that the thermal properties are tunable for magnetically polarizable nanofluids that consist of a colloidal suspension of magnetite nanoparticles. Moreover, the effective thermal conductivity depends also on other mechanisms of particle motion; the commonly explained physics are as follows.

#### *2.3.3.1 Dispersion of the suspended particles*

Dispersion is a system in which particles are dispersed in a continuous phase of a different composition. Surface-active substances (surfactants) can increase the kinetic stability of emulsions greatly so that, once formed, the emulsion does not change significantly over years of storage. Some of the surfactants are thiols, oleic acid, laurate salts, etc. Pak and Cho (1998), Xuan and Li (2000) and others claimed that the abnormal increase in thermal conductivity is due to uniform dispersion of the nanoparticles.

### *2.3.3.2 Intensification of turbulence*

Even though thermal conductivity ( $k_{th}$ ) is a function of primary variables such as thermodynamic pressure and temperature, in a turbulent flow the effective thermal conductivity ( $k_{th} + k_{turb}$ ) due to the effects of turbulent eddies is many times higher than the actual value of  $k_{th}$ . Similarly in nanofluids, such intensification is believed to be possible due to the addition of nanoparticles. However, due to the particle size, the effects of both dispersion and turbulence are negligible and not sufficient to explain the enhancement of thermal conductivity in Nanofluids (Godson, et al., 2010).

### *2.3.3.3 Brownian motion*

It is a seemingly random movement of particles suspended in a liquid or gas and the motion is due to collisions with base fluid molecules, which makes the particles undergo random-walk motion. Thus, the Brownian motion intensifies with an increase in temperature as per the kinetic theory of particles. The potential mechanism for enhancement of thermal conductivity is the transfer of energy due to the collision of higher temperature particles with lower ones (Godson, et al., 2010). The effectiveness of the Brownian motion decreases with an increase in the bulk viscosity.

### *2.3.3.4 Thermophoresis*

Thermophoresis or the Sore't effect is a phenomenon observed when a mixture of two or more types of motile particles (particles able to move) is subjected to the force of a temperature gradient. The phenomenon is most significant in a natural convection process, where the flow is driven by buoyancy and temperature. The particles travel in the direction of decreasing temperature and the process of heat transfer increases with a decrease in the bulk density.

### 2.3.3.5 Diffusiophoresis

Diffusiophoresis (also called as Osmo-phoresis) occurs when there is a migration of particles from a lower concentration zone to a higher concentration one. However, this is not a favorable condition since the nanofluids may lose their non-agglomeration characteristics. Thus, the resulting fluid will result in a discrete spread in the particle density. The thermal conductivity enhancement ratio is defined as the ratio of the thermal conductivity of the nanofluid to that of the base fluid and this ratio depends on the material, size and shape of the particle, volume concentration and the operating temperature itself. The influence of type of material on thermal conductivity enhancement has no effect for relatively low thermal conductivity particles and positive enhancement with higher thermal conductivity particles. For instance, the enhancement of thermal conductivity using metal particles is higher than the metal oxide particles. However, it is difficult to create metal particle nanofluids without particles oxidizing during the production process. A major obstacle for metal-particle nanofluids is eliminating the oxidation process during production and later during usage. Particle coating is one technique that has received some attention to solve this problem.

The smaller in particle size higher will be the enhancement. Since the surface to volume ratio will be higher for small diameter particles which results in uniform distribution of particles gives and the best enhancement. The most commonly used geometric shape of the particles is spherical and cylindrical. The cylindrical particles show an increase in thermal conductivity enhancement due to a mesh formed by the elongated particles that conducts heat through the fluid. This indicates the elongated particles are superior to spherical for thermal conductivity (Trisaksri & Wongwises, 2007). The thermal conductivity enhancement increases with increased particle volume concentration. Metal oxide particle volume concentrations below  $\phi = 4\text{--}5\%$  produces an enhancement level up to about 30% is typical and metal particles with less than  $\phi < 1.5\%$  gives an

enhancement up to 40%. The thermal conductivity of nanoparticles is more temperature sensitive than that of the base fluid.

### **2.3.4 Computational Fluid Dynamics (CFD)**

Computational fluid dynamics or CFD is the analysis of systems involving fluid flow, heat transfer and associated phenomena such as chemical reactions by means of computer-based simulation. The technique is very powerful and spans a wide range of industrial and non-industrial application areas. Some examples are:

- aerodynamics of aircraft and vehicles: lift and drag
- hydrodynamics of ships
- power plant: combustion in internal combustion engines and gas turbines
- turbomachinery: flows inside rotating passages, diffusers etc.
- electrical and electronic engineering: cooling of equipment including microcircuits
- chemical process engineering: mixing and separation, polymer molding
- external and internal environment of buildings: wind loading and heating/ventilation
- marine engineering: loads on off-shore structures
- environmental engineering: distribution of pollutants and effluents
- hydrology and oceanography: flows in rivers, estuaries, oceans
- meteorology: weather prediction
- biomedical engineering: blood flows through arteries and veins

CFD codes are structured around the numerical algorithms that can tackle fluid flow problems. In order to provide easy access to their solving power all commercial CFD packages include sophisticated user interfaces to input problem parameters and to

examine the results. Hence all codes contain three main elements: (i) a pre-processor, (ii) a solver and (iii) a post-processor. Briefly they are examined the function of each of these elements within the context of a CFD code (Versteeg & Malalasekera, 2007).

### 2.3.5 Finite Volume Method Principles

The governing equations were discretized based on a fully conservative finite-volume method using collocated, non-orthogonal, boundary-fitted grids. The domain under consideration was divided into a number of contiguous and non-overlapping control volumes of volume  $V$  bounded by cell faces  $S_j$  as shown in Figure 2.3. The cell-centered approach was used, where the computational nodes were placed at the center of each CV. The boundary nodes and the nodes on the solid-liquid interface, needed for implementation of boundary conditions and the Stefan condition, respectively, were placed at the center of boundary CV faces, Figure 2.4. However, the overall formulation is briefly presented here for the sake of completeness.

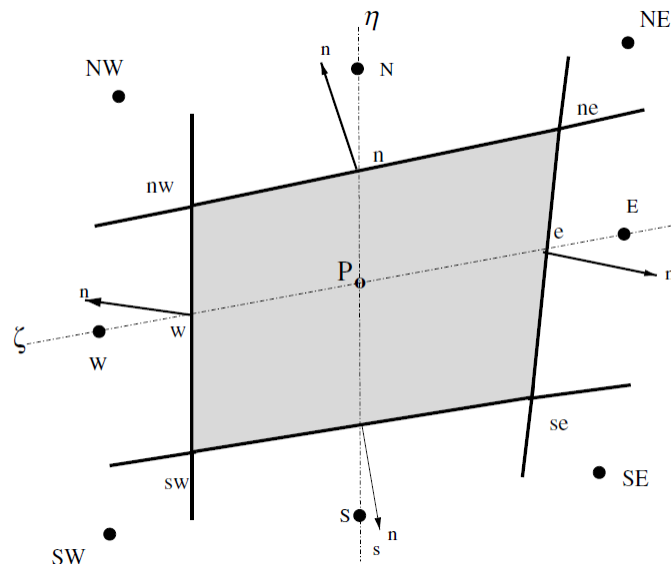
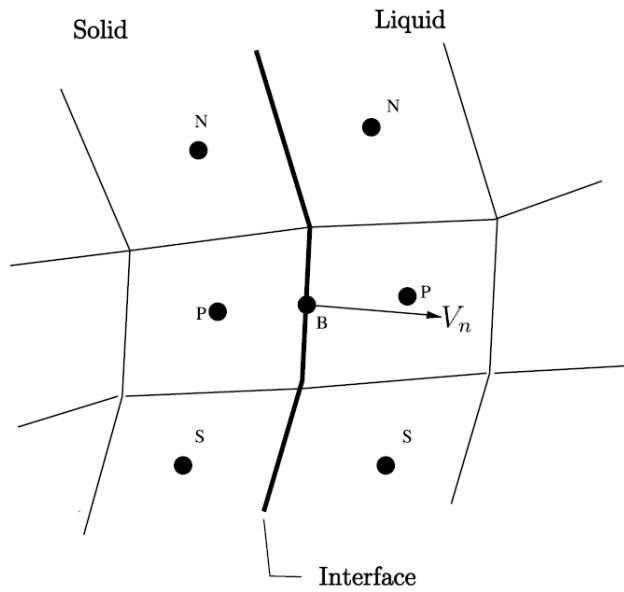
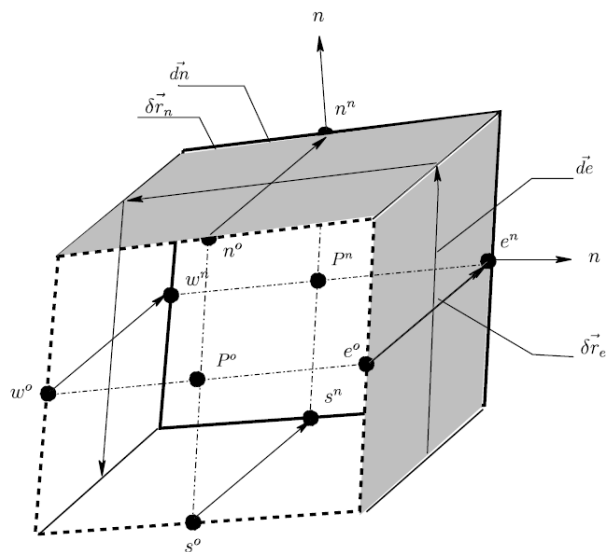


Figure 2.3 A typical 2D generalized control volume (Jana, Ray, & Durst, 2007)



**Figure 2.4 Numerical treatment of control volumes adjacent to interface and its movement (Jana, et al., 2007)**



**Figure 2.5 Movement of typical 2D generalized control volume using cell centered approach (Jana, et al., 2007)**

A fully implicit temporal differentiation was used and the time step  $\delta t$  was first chosen. As has been shown, the space conservation equation, given in Equation (2.1), may be solved explicitly and the grid velocities,  $U_{g,i}$ , at each of the control volume faces may be obtained. In other words, one may use this equation to calculate volume fluxes

through the CV faces which result from the motion of the respective boundaries (Jana, et al., 2007).

Once the new positions of control volumes (Figure 2.5) have been obtained, these volume fluxes and hence the boundary velocities that satisfy the space conservation law, can be easily computed. Substituting these boundary velocities, one may rewrite the space conservation equation as

$$\frac{d}{dt} \int_V dV - \sum_i \int_{S_j} U_{g,i} dS_j = 0, \quad j = e, w, n, s. \quad (2.1)$$

In the discretized form, the space conservation law may also be written as

$$\frac{V^n - V^o}{\delta t} = \frac{\sum_j \delta V_j}{\delta t} = \sum_j (U_{g,i} S_i)_j \quad (2.2)$$

where  $\delta V_j$  represents the volume swept by the  $j$ th face of the CV during time  $\delta t$ , as indicated by the shaded area in Figure 2.5. From the Stefan condition for energy balance at the solid–liquid interface, the coordinates of the CV vertices, lying on the interface, were obtained at a new time level. Numerical grids in both the solid and liquid domains were then recreated. In this manner, the new and the old locations for all the CV vertices were obtained. From this knowledge, the volume swept by the “e” cell face, for example, during time  $\Delta t$  was obtained as

$$\frac{(\delta V_e)_G}{\Delta t} = \frac{1}{\Delta t} (\delta \vec{r}_e \times \delta \vec{d}_e) \quad (2.3)$$

where  $\delta \vec{r}_e$  and  $\delta \vec{d}_e$  are vectors, as shown in Figure 2.5.

In a sequential solution method, the net mass fluxes were considered to be known for all the conservation equations other than the continuity equation and, hence, the mass fluxes in these equations were treated as if they were on a stationary grid. Therefore, the net mass flux,  $\dot{m}_e$ , through a cell face “e”, for example, was calculated as

$$\dot{m}_e = \int_{S_e} (U_i - U_{g,i}) dS_i \quad (2.4)$$

However, in this approach, the mass conservation equation requires special attention and the unsteady term has to be treated in a way which is consistent with the space conservation law. For a fluid of constant density, the mass conservation equation may be written as

$$\frac{d}{dt} \int_V dV - \int_S U_{g,i} dS_i + \int_S U_i dS_i = 0 \quad (2.5)$$

The first two terms in the above equation represent the space conservation law, hence they may be dropped. This leads to the following continuity constraint

$$\int_S U_i dS_i = 0 \quad (2.6)$$

The above discretization method ensured that the unsteady term and the mass fluxes due to grid velocities satisfied the space conservation equation and a strict mass conservation law was obtained (Jana, et al., 2007).

### 2.3.5.1 Advantages and Disadvantages

Finite volume method is a strong, multi-purpose tool for solving variety of scientific and engineering problems due to its organized principals. These characters will let programmers to build fully or partly general-task software which are applicable to different problems with no or less modifications. Finite volume method has the ability to be explained as physical expressions or robust mathematical fundamental. Therefore, implementation of FVM on any problems will be facilitated by understanding underneath basics of the problem's physics while the accuracy of results will be guaranteed by applying convenient mathematical expressions. The domain containing more than two materials can be easily handled by giving different group of elements different material properties. Moreover, assigning variety to properties inside one particular element is possible by defining proper polynomial. Finite volume method can

be dealt with complicated geometries easily and is able to cope with nonlinear or dynamics phenomena. While boundary conditions will be just defined on the whole structure rather than all elements individually, there will be no requirements for in-volume boundary condition considerations. Therefore, because of defining the boundary conditions not in each finite element equations, with any change in boundary conditions the field variable still will be constant. Finite volume method has the ability of dealing with multi-dimensional, continuous domain. So, separate interpolation procedure for having the estimated solution for every node in the domain is not demanded. FVM does not have any need for trial pre-solutions which require to be implemented for the complete multi-dimensional domain. The more realistic results of the solution need more accuracy in the properties of assign material. The deficiency of finite volume method is that the solution is sensitive to defined element properties such as type, form, direction, number and size. When FVM is implemented on computers, comparatively large amount of memory as well as time is taken. After all, the result of solution is accompanied with other data which detecting and separating of needed results from other is troublesome (Versteeg & Malalasekera, 2007).

### Chapter 3: Methodology

Consider a two-dimensional enclosure of height  $H$  and width  $L$  filled with a nanofluid as shown in Figure 3.1. The horizontal walls are assumed to be insulated, non-conducting, and impermeable to mass transfer.

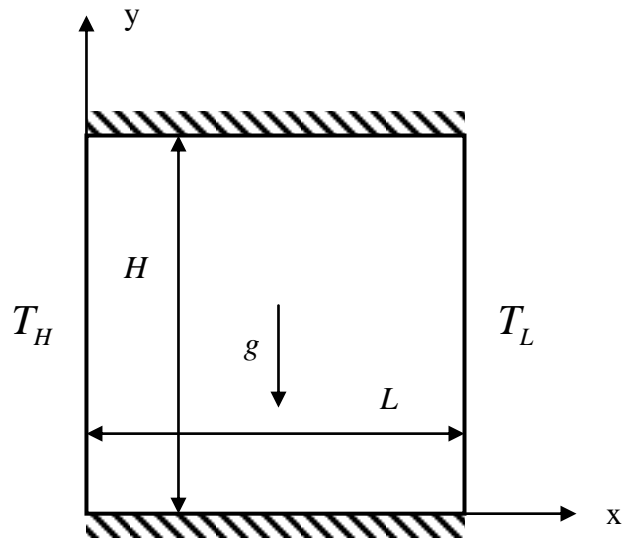


**Figure 3.1 Schematic for the physical model (Khanafer, et al., 2003)**

The nanofluid in the enclosure is Newtonian, incompressible and laminar. The nanoparticles are assumed to have a uniform shape and size as well as homogenous. Moreover, it is assumed that both the fluid phase and nanoparticles are in thermal equilibrium state and they flow at the same velocity. The left vertical wall is maintained at a high temperature ( $T_H$ ) while the right vertical wall is kept at a low temperature ( $T_L$ ). The thermophysical properties of the nanofluid are assumed to be constant except for the density variation in the buoyancy force, which is based on the Boussinesq approximation.

### 3.1 Boundary Conditions

Based on literature (Khanafer, et al., 2003) and in order to be consist on results comparison the initial and boundary conditions for this study are presented as:

$$u = v = T = 0 \text{ for } t = 0 \quad (3.1)$$

$$\left. \begin{aligned} u = v = \frac{\partial T}{\partial y} = 0 & \quad \text{at } y = 0, H \text{ and } 0 \leq x \leq L \\ T = T_H, u = v = 0 & \quad \text{at } x = 0, 0 \leq y \leq H \\ T = T_L, u = v = 0 & \quad \text{at } x = L, 0 \leq y \leq H \end{aligned} \right\} \text{ for } t > 0 \quad (3.2)$$

### 3.2 Governing Equations

The governing equations for the present study taking into the account the above mentioned assumptions are written in dimensional form as

*Continuity equation*

$$\frac{\partial u}{\partial x} + \frac{\partial v}{\partial y} = 0 \quad (3.3)$$

*X-momentum equation*

$$\frac{\partial u}{\partial t} + u \frac{\partial u}{\partial x} + v \frac{\partial u}{\partial y} = \frac{1}{\rho_{nf}} \left( -\frac{\partial p}{\partial x} + \mu_{nf} \nabla^2 u + (\rho\beta)_{nf} g_x (T - T_{ref}) \right) \quad (3.4)$$

*Y-momentum equation*

$$\frac{\partial v}{\partial t} + u \frac{\partial v}{\partial x} + v \frac{\partial v}{\partial y} = \frac{1}{\rho_{nf}} \left( -\frac{\partial p}{\partial y} + \mu_{nf} \nabla^2 v + (\rho\beta)_{nf} g_y (T - T_{ref}) \right) \quad (3.5)$$

*Energy equation*

$$\frac{\partial T}{\partial t} + u \frac{\partial T}{\partial x} + v \frac{\partial T}{\partial y} = \frac{\partial}{\partial x} \left[ \frac{(k_{nf0} + k_d)}{(\rho c_p)_{nf}} \frac{\partial T}{\partial x} \right] + \frac{\partial}{\partial y} \left[ \frac{(k_{nf0} + k_d)}{(\rho c_p)_{nf}} \frac{\partial T}{\partial y} \right] \quad (3.6)$$

The effective density of a fluid containing suspended particles at a reference temperature is given by

$$\rho_{nf} = (1-\phi)\rho_f + \phi\rho_s \quad (3.7)$$

where  $\rho_f$ ,  $\rho_s$ , and  $\phi$  are the density of clear fluid, density of the particles, and the volume fraction of the nanoparticles, respectively. Whereas the heat capacitance of the nanofluid and part of the Boussinesq term are:

$$(\rho c_p)_{nf} = (1-\phi)(\rho c_p)_f + \phi(\rho c_p)_s \quad (3.8)$$

$$(\rho\beta)_{nf} = (1-\phi)(\rho\beta)_f + \phi(\rho\beta)_s \quad (3.9)$$

with  $\phi$  being the volume fraction of the solid particles and subscripts f, nf and s stand for base fluid, nanofluid and solid, respectively.

The effective viscosity of a fluid of viscosity  $\mu_f$  containing a dilute suspension of small rigid spherical particles is given by Brinkman (1952) as

$$\mu_{eff} = \frac{\mu_f}{(1-\phi)^{2.5}} \quad (3.10)$$

The effective stagnant thermal conductivity of the solid–liquid mixture was introduced by Wasp (1979) as follows

$$\frac{k_{nf0}}{k_f} = \frac{k_s + 2k_f - 2\phi(k_f - k_s)}{k_s + 2k_f + \phi(k_f - k_s)} \quad (3.11)$$

This equation is applicable for the two-phase mixture containing micro-sized particles. In the absence of any convenient formula for the calculations of the stagnant thermal conductivity of nanofluids, Eq. (3.11) may approximately apply to obtain a reasonable estimation.

The effective thermal conductivity of the nanofluid may take the following form

$$k_{eff} = k_{nf0} + k_d \quad (3.12)$$

Therefore, the enhancement in the thermal conductivity due to the thermal dispersion is given as (Amiri & Vafai, 1994)

$$k_d = C(\rho c_p)_{nf} |\vec{V}| \phi d_p \quad (3.13)$$

where  $|\vec{V}| = \sqrt{u^2 + v^2}$  and C is an unknown constant which should be determined by matching experimental data.

### 3.3 Computational Solution Methods

In this work the selected solution method for pressure-velocity coupling was SIMPLE (Semi-Implicit Method for Pressure Linked Equations) scheme which the gradient is based on Green-Gauss based cell and pressure is adopted with PRESTO while QUICK method was applied for solving momentum and energy equations. Solution control options for the under relaxation factors were as pressure correction of 0.3, momentum correction of 0.5, liquid fraction of 0.9, thermal energy of 1 in monitoring section, part residuals of  $1 \times 10^{-7}$  for continuity/momentum and  $1 \times 10^{-9}$  for thermal energy in order to satisfy convergence criteria. Number of iterations for every time step was 500.

Special practices related to the discretization of the momentum and continuity equations and their solution by means of the segregated solver are addressed. These practices are most easily described by considering the steady-state continuity and momentum equations in integral form:

$$\oint \rho \vec{v} \cdot d\vec{A} = 0 \quad (3.14)$$

$$\oint \rho \vec{v} \vec{v} \cdot d\vec{A} = -\oint p I \cdot d\vec{A} + \oint \bar{\tau} \cdot d\vec{A} + \int_V \vec{F} dV \quad (3.15)$$

where I is the identity matrix,  $\bar{\tau}$  is the stress tensor, and  $\vec{F}$  is the force vector (Ansys/Fluent, 2009).

### 3.3.1 Discretization of the Momentum Equation

The discretization scheme described in previous section for a scalar transport equation is also used to discretize the momentum equations. For example, the  $x$ -momentum equation can be obtained by setting  $\phi = u$ :

$$a_p u = \sum_{nb} a_{nb} u_{nb} + \sum p_f A \cdot \hat{i} + S \quad (3.16)$$

If the pressure field and face mass fluxes were known, Equation (3.16) could be solved in the manner outlined in the previous section, and a velocity field obtained. However, the pressure field and face mass fluxes are not known a priori and must be obtained as a part of the solution. There are important issues with respect to the storage of pressure and the discretization of the pressure gradient term; these are addressed next.

FLUENT uses a co-located scheme, whereby pressure and velocity are both stored at cell centers. However, Equation (3.16) requires the value of the pressure at the face between adjacent cells. Therefore, an interpolation scheme is required to compute the face values of pressure from the cell values (Ansys/Fluent, 2009).

#### 3.3.1.1 Pressure Interpolation Schemes

The default scheme in FLUENT interpolates the pressure values at the faces using momentum equation coefficients. This procedure works well as long as the pressure variation between cell centers is smooth.

When there are jumps or large gradients in the momentum source terms between control volumes, the pressure profile has a high gradient at the cell face, and cannot be interpolated using this scheme. If this scheme is used, the discrepancy shows up in overshoots/undershoots of cell velocity.

Flows for which the standard pressure interpolation scheme will have trouble include flows with large body forces, such as in strongly swirling flows, in high-Rayleigh-number natural convection and the like. In such cases, it is necessary to pack the mesh in regions of high gradient to resolve the pressure variation adequately (Ansys/Fluent, 2009).

Another source of error is that FLUENT assumes that the normal pressure gradient at the wall is zero. This is valid for boundary layers, but not in the presence of body forces or curvature. Again, the failure to correctly account for the wall pressure gradient is manifested in velocity vectors pointing in/out of walls.

Several alternate methods are available for cases in which the standard pressure interpolation scheme is not valid (Ansys/Fluent, 2009):

- The linear scheme computes the face pressure as the average of the pressure values in the adjacent cells.
- The second-order scheme reconstructs the face pressure in the manner used for second-order accurate convection terms. This scheme may provide some improvement over the standard and linear schemes, but it may have some trouble if it is used at the start of a calculation and/or with a bad mesh. The second order scheme is not applicable for flows with discontinuous pressure gradients imposed by the presence of a porous medium in the domain or the use of the VOF or mixture model for multiphase flow.
- The body-force-weighted scheme computes the face pressure by assuming that the normal gradient of the difference between pressure and body forces is constant. This works well if the body forces are known a priori in the momentum equations (e.g., buoyancy and axisymmetric swirl calculations).

- The PRESTO! (PREssure STAggering Option) scheme uses the discrete continuity balance for a "staggered" control volume about the face to compute the "staggered" (i.e., face) pressure. This procedure is similar in spirit to the staggered-grid schemes used with structured meshes. Note that for triangular and tetrahedral meshes, comparable accuracy is obtained using a similar algorithm.

### 3.3.2 Discretization of the Continuity Equation

Equation (3.14) may be integrated over the control volume to yield the following discrete equation:

$$\sum_f^{N_{faces}} J_f A_f = 0 \quad (3.17)$$

where  $J_f$  is the mass flux through face  $f$ ,  $\rho v_n$ .

The momentum and continuity equations are solved sequentially. In this sequential procedure, the continuity equation is used as an equation for pressure. However, pressure does not appear explicitly in Equation (3.17) for incompressible flows, since density is not directly related to pressure. The SIMPLE (Semi-Implicit Method for Pressure-Linked Equations) family of algorithms is used for introducing pressure into the continuity equation (Ansys/Fluent, 2009).

In order to proceed further, it is necessary to relate the face values of velocity,  $\vec{v}_n$ , to the stored values of velocity at the cell centers. Linear interpolation of cell-centered velocities to the face results in unphysical checker-boarding of pressure. FLUENT uses a procedure similar to Rhie-Chow method to prevent checker boarding. The face value of velocity is not averaged linearly; instead, momentum-weighted averaging, using weighting factors based on the  $a_p$  coefficient from Equation (3.16), is performed.

Using this procedure, the face flux,  $J_f$ , may be written as

$$J_f = \hat{J}_f + d_f (p_{c0} - p_{c1}) \quad (3.18)$$

where  $p_{c0}$  and  $p_{c1}$  are the pressures within the two cells on either side of the face, and  $\hat{J}_f$  contains the influence of velocities in these cells.

The term  $d_f$  is a function of  $a_p$ , the average of the momentum equation  $a_p$  coefficients for the cells on either side of face  $f$ .

### 3.3.2.1 Density Interpolation Schemes

For compressible flow calculations (i.e., calculations that use the ideal gas law for density), FLUENT applies upwind interpolation of density at cell faces. (For incompressible flows, FLUENT uses arithmetic averaging.) Three interpolation schemes are available for the density upwinding at cell faces: first-order upwind (default), second-order-upwind, and QUICK.

The first-order upwind scheme sets the density at the cell face to be the upstream cell-center value. This scheme provides stability for the discretization of the pressure-correction equation, and gives good results for most classes of flows. The first-order scheme is the default scheme for compressible flows.

The second-order upwind scheme provides stability for supersonic flows and captures shocks better than the first-order upwind scheme. The QUICK scheme for density is similar to the QUICK scheme used for other variables (Ansys/Fluent, 2009). The second-order upwind and QUICK schemes for density are not available for compressible multiphase calculations; the first-order upwind scheme is used for the compressible phase, and arithmetic averaging is used for the incompressible phases.

### 3.3.3 Pressure-Velocity Coupling

Pressure-velocity coupling is achieved by using Equation (3.18) to derive an equation for pressure from the discrete continuity Equation (3.17). FLUENT provides the option to choose among pressure velocity coupling algorithms such as SIMPLE (Ansys/Fluent, 2009).

#### 3.3.3.1 SIMPLE Solution Algorithm

Many numerical methods for solving the 2D Navier-Stokes equation in the literature are tested using the 2D driven cavity problem. In this research project SIMPLE algorithm is used with primitive variables velocity and pressure. The multi-grid method and vorticity stream function formulation being implemented. The use of simple iterative techniques to solve the Navier-Stokes equations might lead to slow convergence. The rate of convergence is also generally strongly dependent on parameters such as Reynolds number and mesh size.

Semi-Implicit Method for Pressure-Linked Equations was first proposed by Patankar (1980). It will start with the discrete continuity equation and substitute into this the discrete  $u$  and  $v$  momentum equations containing the pressure terms resulting in an equation for discrete pressures. SIMPLE actually solves for a relative quantity called pressure correction. It predicts an initial flow field and pressure distribution in the domain (Figure 3.2). The set of momentum and continuity equations are coupled and are nonlinear so the equations are being solved iteratively. The pressure field is assumed to be known from the previous iteration. Using this  $u$  and  $v$  momentum equations are solved for the velocities. At this stage the newly obtained velocities do not satisfy continuity since the pressure field assumed is only a prediction. Corrections to velocities and pressure are proposed to satisfy the discrete continuity equation (Ambatipudi, 2006).

$$u = u^* + u' \quad (3.19)$$

$$v = v^* + v' \quad (3.20)$$

$$p = p^* + p' \quad (3.21)$$

where  $u^*$ ,  $v^*$  and  $p^*$  are the guess values and  $u'$ ,  $v'$  and  $p'$  are the corrections. The simple algorithm also requires the corrected velocities and pressures to satisfy the momentum equations leading to the corrected momentum equations.

$$a_e u'_e = \sum_{nb} a_{nb} u'_{nb} + \Delta y (p'_P - p'_E) \quad (3.22)$$

$$a_n v'_n = \sum_{nb} a_{nb} v'_{nb} + \Delta x (p'_S - p'_P) \quad (3.23)$$

Approximations to the velocity correction are made by ignoring the  $\sum_{nb} a_{nb} u'_{nb}$  and  $\sum_{nb} a_{nb} v'_{nb}$ . Substituting these corrected velocities into the continuity equations yields a discrete pressure correction equation.

$$a_P p'_P = \sum_{nb} a_{nb} p'_{nb} + b \quad (3.24)$$

$$a_E = \rho_e d_e \Delta y \quad (3.25)$$

$$a_W = \rho_w d_w \Delta y \quad (3.26)$$

$$a_W = \rho_w d_w \Delta y \quad (3.27)$$

$$a_N = \rho_n d_n \Delta x \quad (3.28)$$

$$a_S = \rho_s d_s \Delta x \quad (3.29)$$

$$a_P = \sum_{nb} a_{nb} \quad (3.30)$$

$$b = F_w^* - F_e^* + F_s^* - F_n^* \quad (3.31)$$

where  $d_i = \frac{\Delta y}{a_i}$  and  $F_i^* = \rho u_i^* \Delta y$  for  $e$ ,  $w$ ,  $n$  and  $s$ . Here the Scarborough condition is

satisfied only in equality (Ambatipudi, 2006).

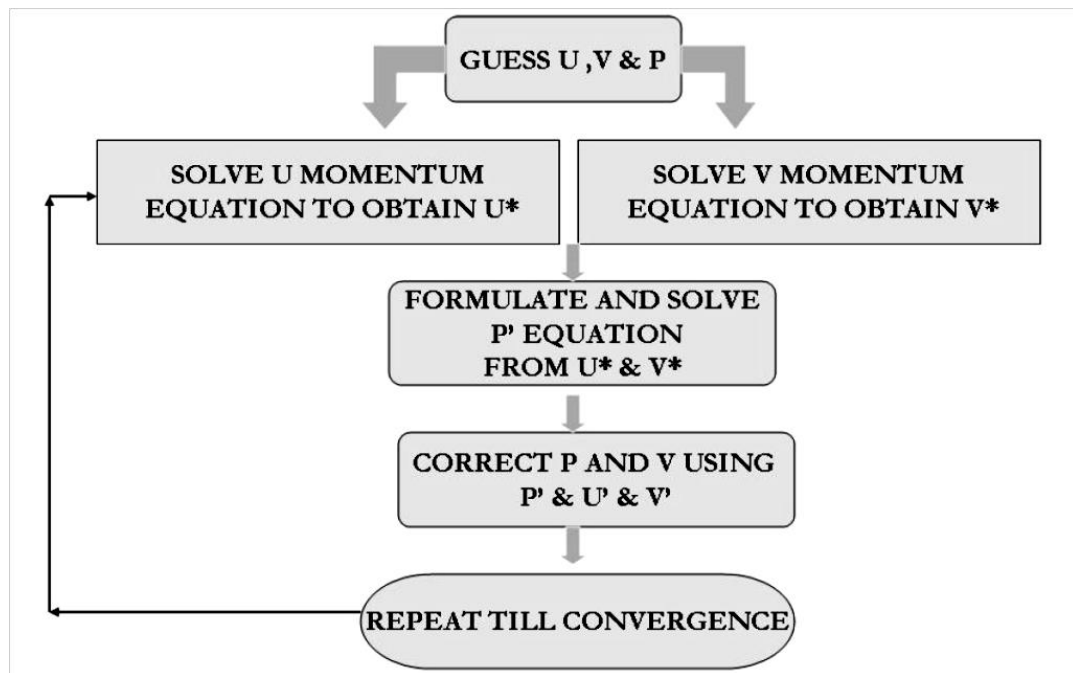


**Figure 3.2** Flow chart showing the SIMPLE Algorithm (Ambatipudi, 2006)

### 3.3.3.2 Under-Relaxation

In numerical analysis of fluid flow and heat transfer problems, iterative methods are frequently adopted in which velocity components are solved in segregated manner and the linkage between velocity and pressure is ensured by the SIMPLE-series algorithm. Since, the leading iterative approach SIMPLE was proposed (Patankar, 1980), it has been widely applied in the fields of computational fluid dynamics (CFD) and numerical heat transfer (NHT). Over the past three decades, many variants such as SIMPLER, SIMPLEC, SIMPLEX and so on were developed, which consist the so-called SIMPLE-family solution algorithms. During the development of the SIMPLE-family algorithms, how to accelerate the iteration convergence is one of the key problems for enhancing the solution algorithm.

In SIMPLE-family algorithms, the iteration convergence can be accelerated by three methods (Min & Tao, 2007). By applying this explicit correction step to the SIMPLE, SIMPLEC and PISO algorithms, significant reductions in the number of iterations and

CPU time to achieve convergence were demonstrated. The second method is to choose appropriate values of the under-relaxation factors. Patankar (1980) pointed out that for the SIMPLE algorithm the velocity under-relaxation factor of 0.5 and the pressure under-relaxation of 0.8 were found to be satisfactory in a large number of fluid-flow computations. However, it is recommended that if the computational grid is not severely nonorthogonal, the relation:

$$\alpha_u + \alpha_p = c \quad (3.32)$$

gives almost the optimum result, where the constant  $c$  is 1 (Demirbas, 2006) or 1.1 (Min & Tao, 2007). Later a pressure under-relaxation factor based on the minimization of the global residual norm of the momentum equations was proposed (Darzi, Farhadi, & Sedighi, 2012). The procedure was applied to SIMPLE algorithms to automatically select the pressure under-relaxation factor to minimize the global residual norm of the momentum equations at each iteration level, but a notable increase in convergence was not achieved. Some other researchers (Min & Tao, 2007; Patankar, 1980) all stated the need for a method of automatically optimizing the relaxation factors.

## Chapter 4: Results and Discussions

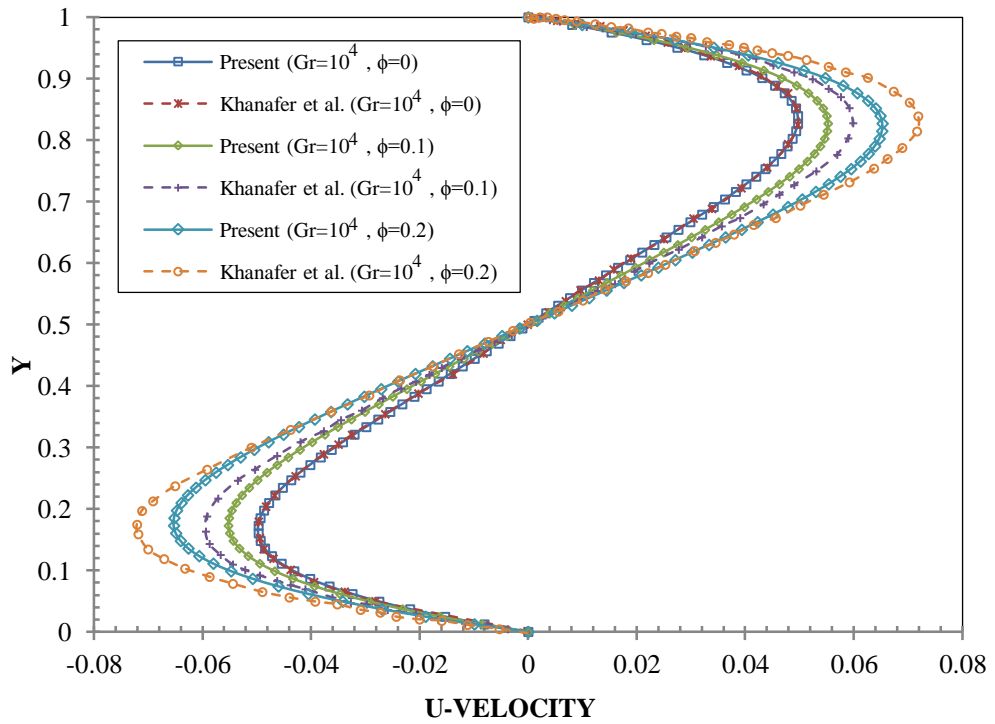
### 4.1 Model Benchmarking

The outcomes of this computational study for natural convection of nanofluids within differentially-heated square cavity has been benchmarked with previous work of Khanafer et al. (2003).

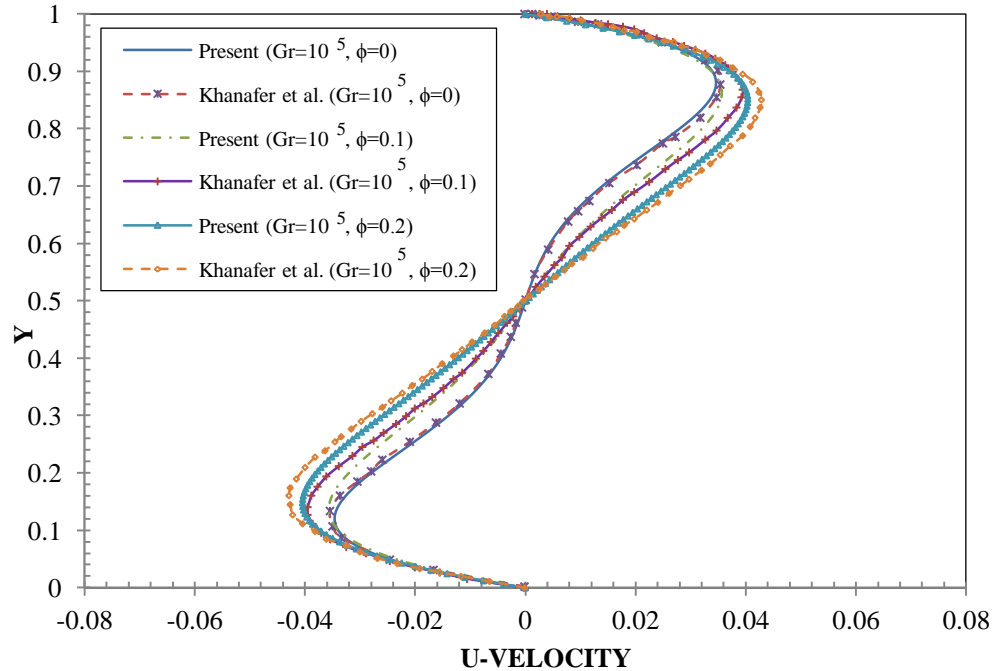
The horizontal velocity module on the vertical mid plane of the square cavity for the present study with  $81 \times 81$  meshing size expected and matched up to Khanafer et al. (2003) in Figure 4.1 and Figure 4.2 for two different Grashof number,  $Gr = 10^4$  and  $Gr = 10^5$ , respectively.

Figure 4.1 shows the comparison of U-velocity components for the base fluid and the nanofluid ( $\phi=0\%$ , 10% and 20%) filled inside square cavity with  $Gr=10^4$ . The present numerical data for the velocity are compared with that of Khanafer et al. (2003). The agreeable results are obtained. As shown in the Figure 4.1, the trend of the horizontal fluid velocity exhibits accelerated flow near the horizontal walls and weak in the center of square cavity which indicate that nanofluids act more similar to a base fluid.

In the comparison graph for the cases of pure fluid for two Grashof number the conformity is great. In addition, the dimensionless velocity for Grashof number of  $Gr = 10^5$  is lower than corresponding dimensionless velocity of Grashof number  $Gr = 10^4$ .



**Figure 4.1 Comparison of the predicted horizontal velocity component on the vertical mid-plane of the square cavity for the present study and those of Khanafar et al. (2003) with  $Gr=10^4$**



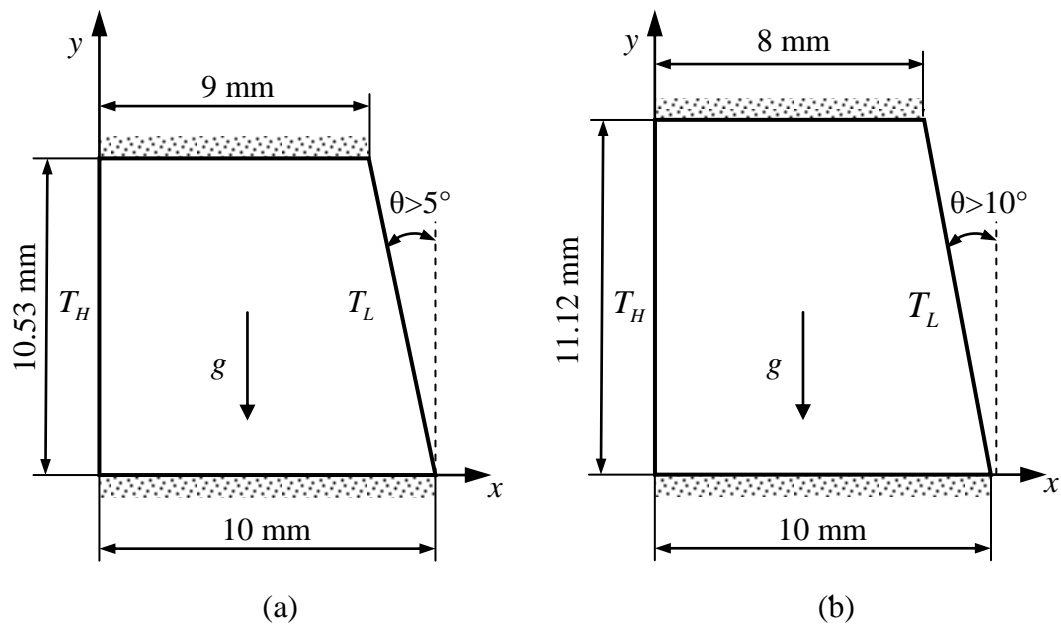
**Figure 4.2 Comparison of the predicted horizontal velocity component on the vertical mid-plane of the square cavity for the present study and those of Khanafar et al. (2003) with  $Gr=10^5$**

Figure 4.2 shows the comparison of U-velocity components for the base fluid and the nanofluid ( $\phi=0\%$ , 10% and 20%) filled inside square cavity with  $Gr=10^5$ . The present numerical data for the velocity are compared with that of Khanafer et al. (2003). The agreeable results are obtained. In the case of base fluid, both velocity components for the present work and that of Khanafer et al. (2003) covering each other.

Adding more nanoparticles, irregular and random motion of solid particles increase the energy and momentum transports all over the cavity (Khanafer, et al., 2003). Raising dispersion can lead to increasing of thermal conductivity.

#### 4.2 Numerically Solved Problem

The aim of this work is to study the effects of nanoparticle volume fraction and shape variations on solidification time. Two trapezoidal shaped geometries are used for this study. It is noted that the internal area of both cavities are kept constant  $100 \text{ mm}^2$ .



**Figure 4.3 Geometry of numerically solved problem**

As illustrated in Figure 4.3 (a), by keeping the lower edge fixed, the upper edge is decreased by 1 mm (from 10 mm to 9 mm). Based on calculations, the side edge and

angle has been determined as 10.53 mm and 5.43°, respectively. Figure 4.3 (b) has the same configuration with upper edge length as 8 mm and height as 11.12 mm with inclination angle of 10.20°. By this method, observing the effect of angle variation with freezing time facilitated as the area remains constant.

On the other hand for underrating of the effect of nanoparticle the work has been done with three different solid particle volume fractions  $\phi$  of 0, 0.1 and 0.2 considered for two different Grashof numbers of  $10^4$  and  $10^5$ .

The geometry is a trapezoidal cavity with area of 100 mm<sup>2</sup>. Meshing is obtained by implementing Uniform Quad Method with element size of 0.12 mm as illustrated in Figure 4.4.

The relevant thermophysical properties of components as well as nanofluids are given in Table 4.1.

**Table 4.1 Thermophysical properties of the copper nanoparticles, water ( $\phi=0$ ) and nanofluids with solid copper nanoparticle volume fractions ( $\phi$ ) equal to 0.1 and 0.2 (Khodadadi & Hosseinizadeh, 2007)**

	Copper nanoparticles	Base fluid $\phi = 0$	Nanofluid 1 $\phi = 0.1$	Nanofluid 2 $\phi = 0.2$
$\rho$ [kg/m <sup>3</sup> ]	8954	997.1	1792.79	2588.48
$\mu$ [Pa s]	-	$8.9 \times 10^{-4}$	$1.158 \times 10^{-3}$	$1.555 \times 10^{-3}$
$c_p$ [J/kg K]	383	4179	2283.107	1552.796
$k$ [W/m K]	400	0.6	0.8	1.04748
$\alpha$ [m <sup>2</sup> /s]	$1.17 \times 10^{-4}$	$1.44 \times 10^{-7}$	$1.95 \times 10^{-7}$	$2.6 \times 10^{-7}$
$\beta$ [1/K]	$1.67 \times 10^{-5}$	$2.1 \times 10^{-4}$	$1.13 \times 10^{-4}$	$7.63 \times 10^{-5}$
$L$ [J/kg]	-	$3.35 \times 10^5$	$1.68 \times 10^5$	$1.03 \times 10^5$
$Pr$	-	6.2	3.31	2.3
$Ste$	-	0.125	0.136	0.150
$\tau_1$ [s]	-	2950	2000	1300
$\tau_2$ [s]	-	3000	2000	1400

Solidification of NEPCMs with respect to time is illustrated in Figure 4.5 to Figure 4.7.

The nanofluid in the cavity is Newtonian, incompressible and laminar. The diameter of the solid copper nanoparticle  $d_p$  is equal 10 nm that suspended in the water that assume as a base fluid. The freezing starts at time  $t=0$ , the temperature of both left and right

edges were decreased by  $10^{\circ}C$  that is below the freezing temperature of the base fluid (water). By keeping the left wall at  $0^{\circ}C$  ( $T_H = 273.15 K$ ) and the right wall at  $-10^{\circ}C$  ( $T_L = 263.15 K$ ) solidification starts from the right wall and pass through cavity to the left wall. The thermophysical properties of nanofluids are assumed to be constant except for density due to the buoyancy force, which is based on the Boussinesq approximation.

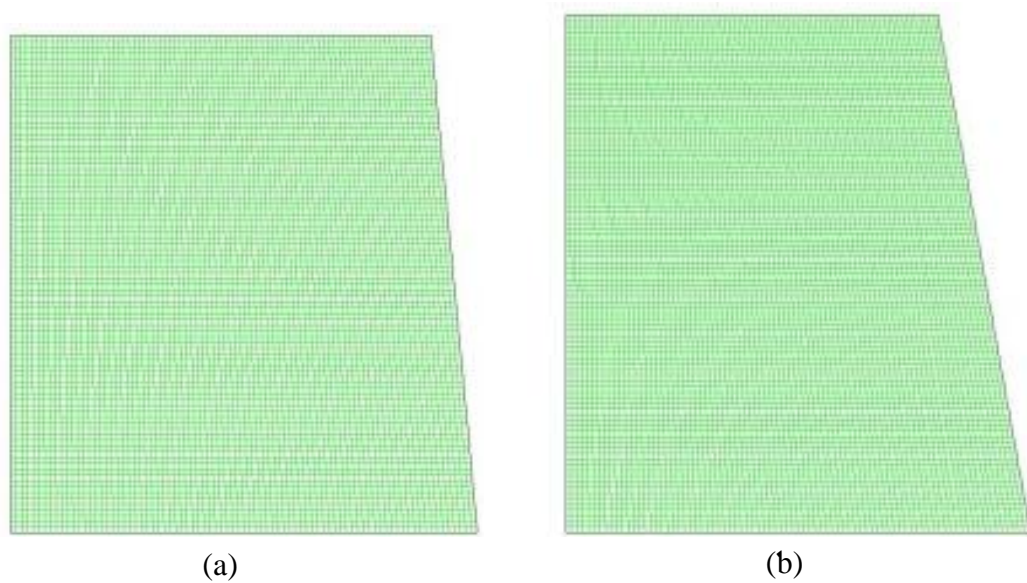


**Figure 4.4 Generated mesh for the shape 1 and shape 2 models of trapezoidal cavity**

The simulation started with modeling the geometry in ANSYS/FLUENT commercial software as a 2D shape in the defining Cartesian coordinate system (X, Y, Z) framework. Afterward, the simulation parameters were set in the Fluent. For the current study the equations are considered as pressure based which is suitable for incompressible flows. Velocities are absolute and time is unsteady or transient because of variations by in time. Gravitational acceleration is in the direction of Y axis with magnitude of  $-9.81 m/s^2$  which can be activated through Gravity option during models. The required parameters of energy equation, solidification and melting were activated accordingly. Mushy zone constant were set to  $1 \times 10^5 kg/m^3s$ . Material definition for water implemented by choosing Boussinesq approximation for density of base fluid (water), specific heat,

thermal conductivity, viscosity, thermal expansion coefficient and pure solvent melting where obtained from Table 4.1. Heat and solidus/ liquidus temperatures were chosen as 273.15 k (0° C). Boundary conditions for top and bottom horizontal walls defined with the heat transfer thermal convection coefficient of 0 W/m<sup>2</sup>.k as they are considered as adiabatic surfaces. Left side wall, hot surface, temperature maintained at 273.15 k and cold right side wall temperature kept in 263.15 k.

#### **4.2.1 Volume Fraction of Solid Particles of $\phi = 0\%$ (Base fluid)**

The freezing of base fluid which is water is shown in the Figure 4.5. Different time intervals were adopted within chosen number of time steps of 3100 seconds. By comparing shape 1 and shape 2 a significant increase in solidification for shape 2 is observed which is due to increase in the angle of trapezoidal that can accelerate the freezing time. Completion of freezing occurs after 2441 seconds for while shape 1 solidified at 2644 seconds.

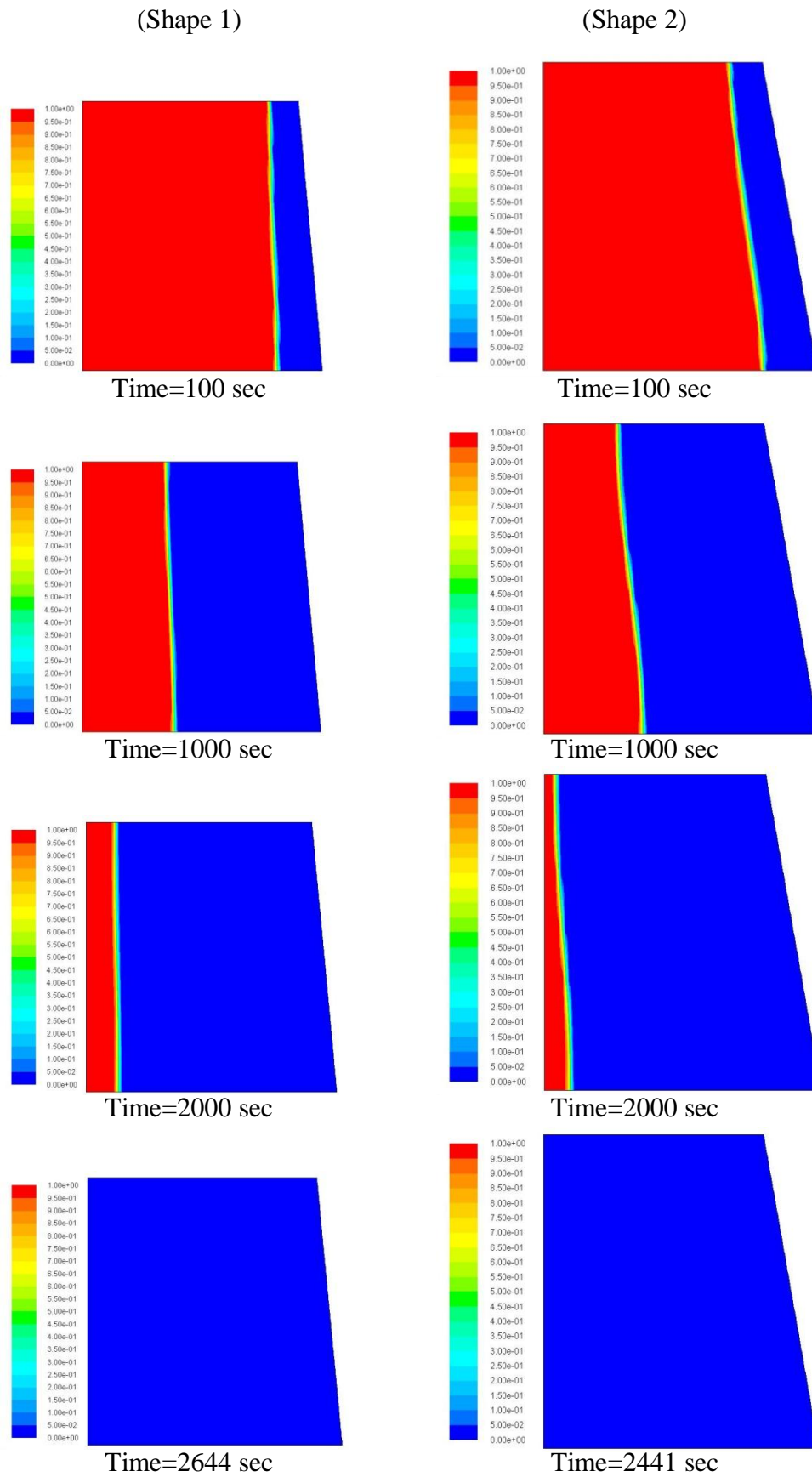


Figure 4.5 Colorized contours of the volume fraction of the nanofluid with  $\phi = 0\%$

#### **4.2.2 Volume Fraction of Solid Particles of $\phi = 10\%$ (Nanofluid 1)**

According to Table 4.1, for the case of nanofluid 1 with  $\phi = 10\%$  the specifications of nanofluid such as density by considering Boussinesq approximation,  $c_p$  for specific heat, thermal conductivity, viscosity, thermal expansion coefficient, and pure solvent melting heat were chosen. Solidus/liquidus temperature was 273.15 K. Number of time steps was set on 2100 seconds. Figure 4.6 shows the related freezing of 0.1 solid particle volume fractions for two trapezoidal shapes that had been done for different simulation time intervals. As it can be observed, for each time there are rising in solidification time with adding nanoparticle due to enhanced thermal conductivity of the nanofluid and smaller value of latent heat. By adding more nanoparticles, freezing time is increased in which for shape 1 the total solidification is at 1810 seconds while for shape 2 the freezing time observed to be about 1676 seconds as a result of angle variation effect. The blue color shows the solid part of the system.

#### **4.2.3 Volume Fraction of Solid Particles of $\phi = 20\%$ (Nanofluid 2)**

For the third case, namely as nanofluid 2 with  $\phi = 20\%$  the defined properties followed as with Boussinesq approximation, specific heat, thermal conductivity, viscosity, thermal expansion coefficient and pure solvent melting heat were taken from Table 4.1 while solidus/liquidus temperature was 273.15 K. Number of time steps were set to 1600 seconds and other factors remained constant.

As displayed in Figure 4.7, by charging more solid particle which means increasing solid particle volume fraction, even faster in freezing time is observed for various times variations.

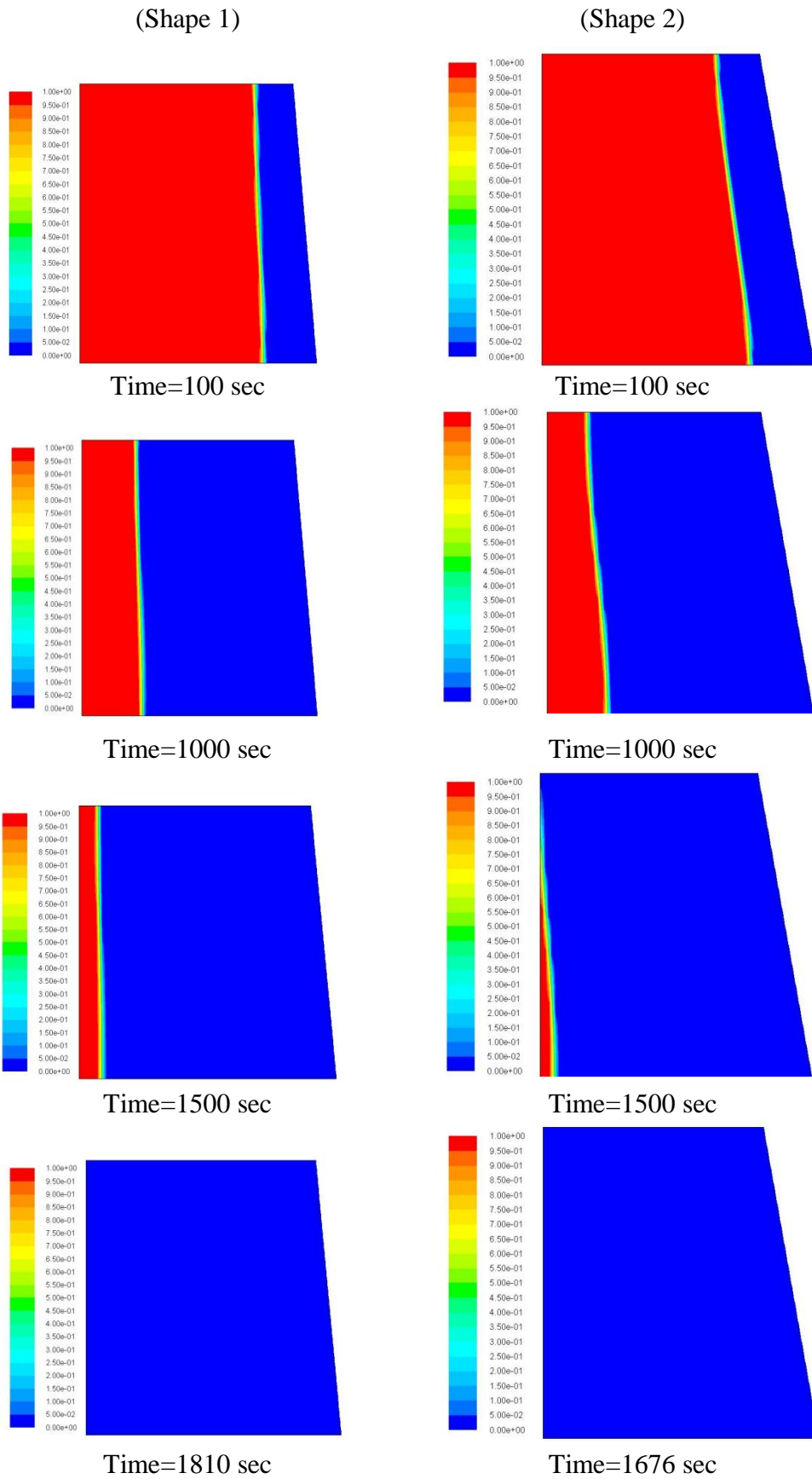


Figure 4.6 Colorized contours of the volume fraction of the nanofluid with  $\phi = 10\%$

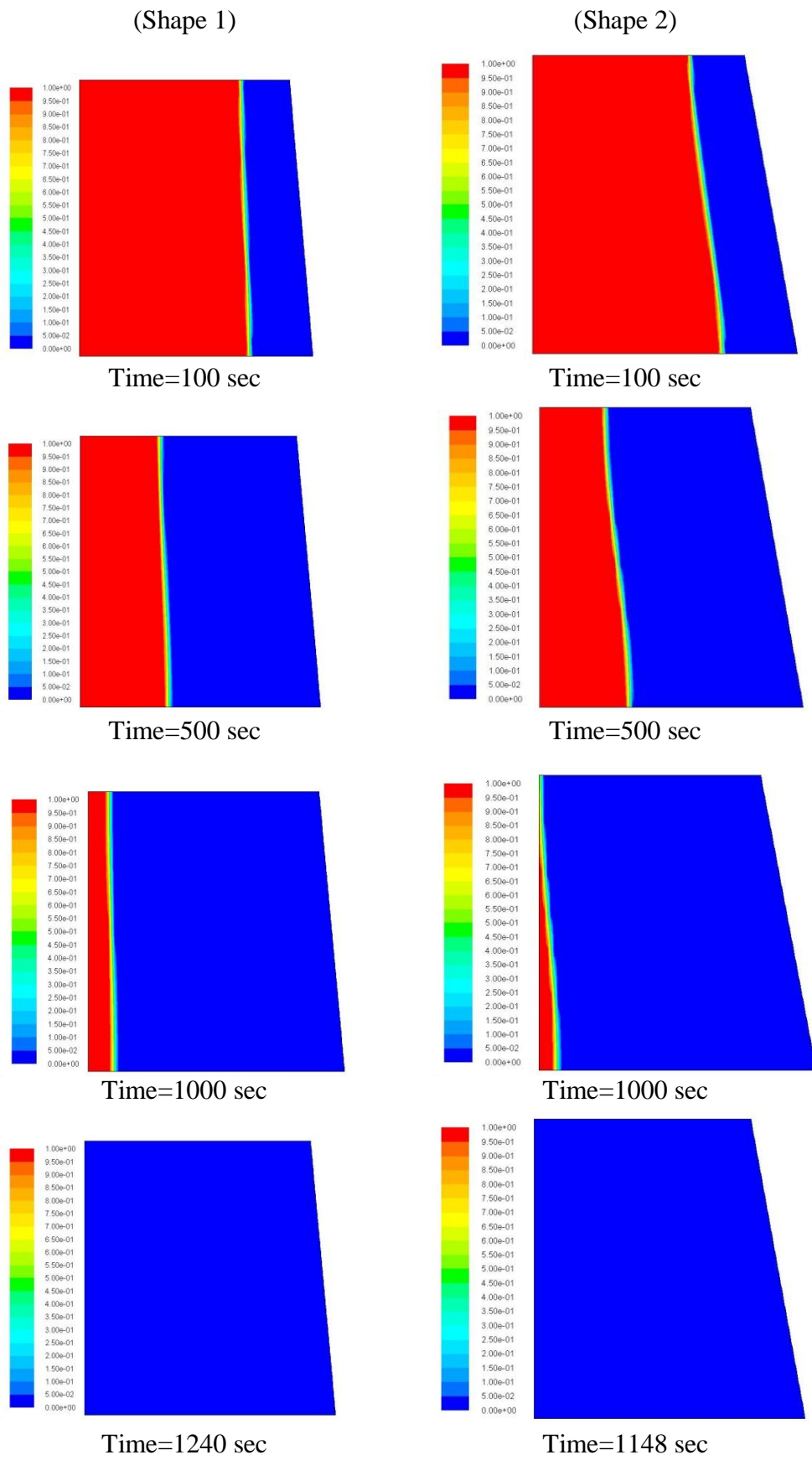


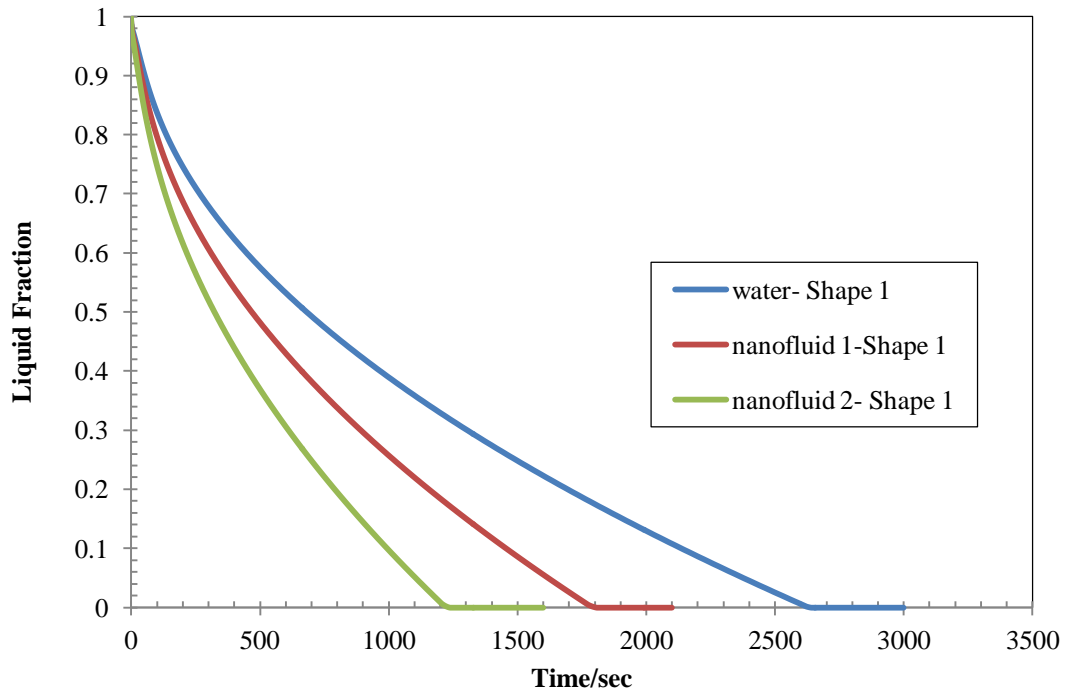
Figure 4.7 Colorized contours of the volume fraction of the nanofluid with  $\phi = 20\%$

The final stage of solidification for this case,  $\phi = 20\%$ , can be observed at 1240 seconds for shape 1 and 1148 seconds for shape 2. Solidification time further decreases.

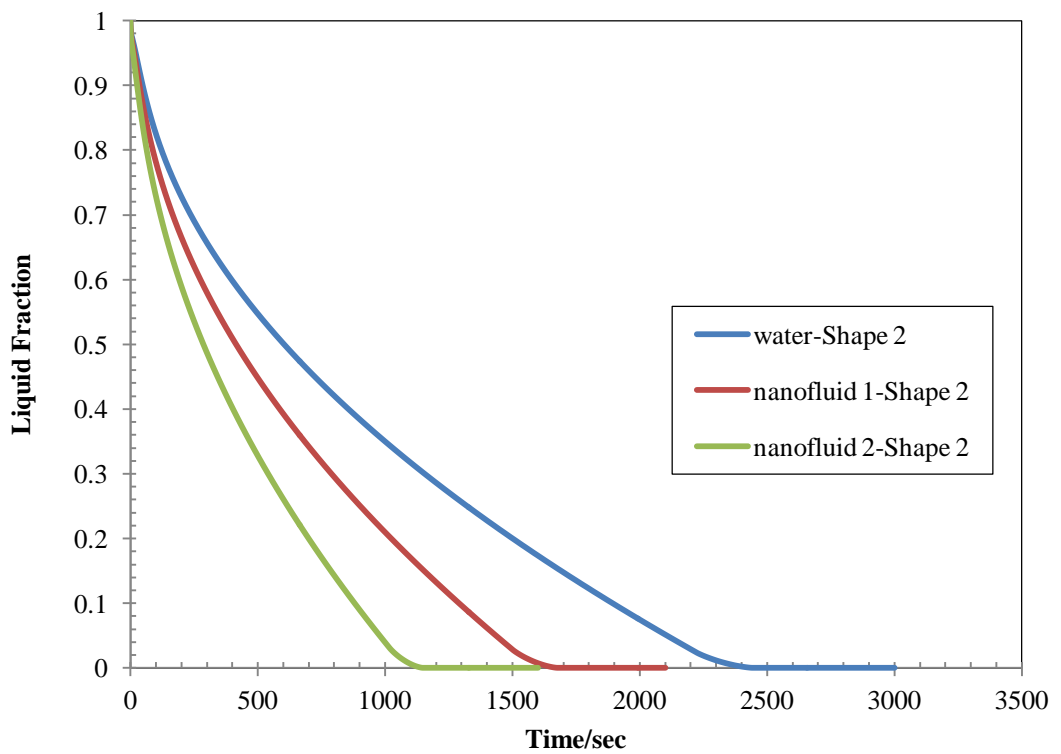
It is evident from the figures that with increasing the nanoparticle volume fraction, NEPCMs will freeze quickly. This phenomenon can be described by the fact that the thermal conductivity of nanofluids were improved by adding nano particles and consequently the latent heat of fusion were lowered which is due to decreased required energy per unit mass of nanofluids for freezing (Khodadadi & Hosseinizadeh, 2007). Higher heat release rate of NEPCM is an obvious sign of excellent potential for thermal energy storage applications.

Figure 4.8 shows the variation of liquid fraction with respect to time for shape 1. As can be seen for water, complete freezing time is 2644 seconds, whereas in order to have complete freezing for  $\phi = 10\%$  the time was 1810 seconds and for  $\phi = 20\%$  the total time was 1240 seconds.

Figure 4.9 shows the variation of liquid fraction with respect to time for shape 2. For base fluid, complete freezing time is 2441 seconds. However, in order to obtain complete freezing for nanofluid 1 ( $\phi = 10\%$ ) the time was 1676 seconds and for nanofluid 2 ( $\phi = 20\%$ ), the total time was 1148 seconds.



**Figure 4.8** Liquid fraction-time comparison graph for Shape 1



**Figure 4.9** Liquid fraction-time comparison graph for Shape 2

## Chapter 5: Conclusions

In summary, nanofluids definition and properties were studied, nanofluids were found to have tremendously enhances on heat transfer characteristics of the base fluid, and is ideally suited for practical applications due to its marvelous characteristics. This research report addresses the unique features of nanofluids, such as enhancement of heat transfer, improvement in thermal conductivity, increase in surface volume ratio, Brownian motion, thermophoresis, etc. Improved functionality of phase change materials (PCM) through dispersion of nanoparticles is reported with preceding application of newly considered geometries as a trapezoidal shape. The problem of natural convection heat transfer in a two-dimensional trapezoidal enclosure filled with nanofluids has been studied numerically. Various inclination angles of the sloping wall, volume fractions, and Grashof numbers have been considered and the flow and temperature fields as well as the heat transfer rate have been analyzed. The results of the numerical analysis lead to the following conclusions:

1. The structure of the fluid flow within the enclosure was found to depend upon, inclination angle of sloping wall and nanoparticles concentration and type.
2. The Cu nanoparticles with high volume fraction ( $\phi = 20\%$ ) combines with an acute sloping wall (Shape 2) as found to be most effective in enhancing performance of heat transfer rate.

It is highly recommended to precede this study combined with experimental studies in order to proof the retrieved data from the computational fluid dynamics (CFD) simulations.

## References

- Abhat, A. (1983). Low temperature latent heat thermal energy storage: Heat storage materials. *Solar energy*, 30(4), 313-332. doi: [http://dx.doi.org/10.1016/0038-092X\(83\)90186-X](http://dx.doi.org/10.1016/0038-092X(83)90186-X)
- Ambatipudi, V. (2006). Simple solver for driven cavity flow problem. *ASME*, 55(4), 13.
- Amiri, A., & Vafai, K. (1994). Analysis of dispersion effects and non-thermal equilibrium, non-Darcian, variable porosity incompressible flow through porous media. *International Journal of Heat and Mass Transfer*, 37(6), 939-954. doi: [http://dx.doi.org/10.1016/0017-9310\(94\)90219-4](http://dx.doi.org/10.1016/0017-9310(94)90219-4)
- Ansys/Fluent. (2009). 12.0 User's Guide. ANSYS Inc.
- Brinkman, H. C. (1952). The viscosity of concentrated suspensions and solutions. *The Journal of Chemical Physics*, 20(4), 571-571.
- Choi, S. U. S. (1995). *Enhancing thermal conductivity of fluids with nanoparticles*.
- Darzi, A. R., Farhadi, M., & Sedighi, K. (2012). Numerical study of melting inside concentric and eccentric horizontal annulus. *Applied mathematical modelling*, 36(9), 4080-4086. doi: <http://dx.doi.org/10.1016/j.apm.2011.11.033>
- Das, S. K., Choi, S. U., Yu, W., & Pradeep, T. (2007). *Nanofluids: Science and Technology*: Wiley.
- Demirbas, M. F. (2006). Thermal energy storage and phase change materials: An overview. *Energy Sources, Part B: Economics, Planning, and Policy*, 1(1), 85-95.
- Dincer, I., & Rosen, M. A. (2011). *Thermal Energy Storage: Systems and Applications*: Wiley.
- Eastman, J. A., Choi, S. U. S., Li, S., Yu, W., & Thompson, L. J. (2001). Anomalously increased effective thermal conductivities of ethylene glycol-based nanofluids containing copper nanoparticles. *Applied Physics Letters*, 78(6), 718-720.
- Fan, L., & Khodadadi, J. (2011). An experimental investigation of enhanced thermal conductivity and expedited unidirectional freezing of cyclohexane-based nanoparticle suspensions utilized as nano-enhanced phase change materials (NePCM). *International Journal of Thermal Sciences*.
- Godson, L., Raja, B., Mohan Lal, D., & Wongwises, S. (2010). Enhancement of heat transfer using nanofluids—an overview. *Renewable and Sustainable Energy Reviews*, 14(2), 629-641.

- Guo, C., & Zhang, W. (2008). Numerical simulation and parametric study on new type of high temperature latent heat thermal energy storage system. *Energy Conversion and Management*, 49(5), 919-927.
- Jana, S., Ray, S., & Durst, F. (2007). A numerical method to compute solidification and melting processes. *Applied mathematical modelling*, 31(1), 93-119.
- Jegadheeswaran, S., & Pohekar, S. D. (2009). Performance enhancement in latent heat thermal storage system: a review. *Renewable and Sustainable Energy Reviews*, 13(9), 2225-2244.
- Kang, C., Okada, M., Hattori, A., & Oyama, K. (2001). Natural convection of water-fine particle suspension in a rectangular vessel heated and cooled from opposing vertical walls (classification of the natural convection in the case of suspension with a narrow-size distribution). *International Journal of Heat and Mass Transfer*, 44(15), 2973-2982. doi: [http://dx.doi.org/10.1016/S0017-9310\(00\)00286-6](http://dx.doi.org/10.1016/S0017-9310(00)00286-6)
- Khanafer, K., Vafai, K., & Lightstone, M. (2003). Buoyancy-driven heat transfer enhancement in a two-dimensional enclosure utilizing nanofluids. *International Journal of Heat and Mass Transfer*, 46(19), 3639-3653.
- Khodadadi, J., & Hosseinizadeh, S. (2007). Nanoparticle-enhanced phase change materials (NEPCM) with great potential for improved thermal energy storage. *International communications in heat and mass transfer*, 34(5), 534-543.
- Kim, J., Kang, Y. T., & Choi, C. K. (2004). Analysis of convective instability and heat transfer characteristics of nanofluids. *Physics of Fluids*, 16(7), 2395-2401.
- Kreith, F., Manglik, R. M., & Bohn, M. S. (2010). *Principles of Heat Transfer*: Cengage Learning.
- Lane, G. A. (1983). *Solar Heat Storage: Background and scientific principles*: CRC Press.
- Lane, G. A. (1986). *Solar heat storage: latent heat materials*: CRC Press.
- Lázaro, A., Zalba, B., Bobi, M., Castellón, C., & Cabeza, L. F. (2006). Experimental study on phase change materials and plastics compatibility. *AIChE Journal*, 52(2), 804-808. doi: 10.1002/aic.10643
- Manca, O., Jaluria, Y., & Poulikakos, D. (2010). Heat transfer in nanofluids. *Advances in Mechanical Engineering*, 2010. doi: 10.1155/2010/380826
- Masuda, H., Ebata, A., Teramae, K., & Hishinuma, N. (1993). Alteration of thermal conductivity and viscosity of liquid by dispersing ultra-fine particles dispersion of Al<sub>2</sub>O<sub>3</sub>, SiO<sub>2</sub> and TiO<sub>2</sub> ultra-fine particles. *Netsu Bussei*, 7(4), 227-233.
- Min, C., & Tao, W. (2007). An under-relaxation factor control method for accelerating the iteration convergence of flow field simulation. *Engineering Computations*, 24(8), 793-813.
- Okada, M., Kang, C., Oyama, K., & Yano, S. (2001). Natural convection of a water-fine particle suspension in a rectangular cell heated and cooled from opposing

- vertical walls: The effect of distribution of particle size. *Heat Transfer—Asian Research*, 30(8), 636-647. doi: 10.1002/htj.1041
- Pak, B. C., & Cho, Y. I. (1998). Hydrodynamic and heat transfer study of dispersed fluids with submicron metallic oxide particles. *Experimental Heat Transfer*, 11(2), 151-170. doi: 10.1080/08916159808946559
- Patankar, S. V. (1980). *Numerical heat transfer and fluid flow*: Hemisphere Publishing Company.
- Philip, J., Laskar, J. M., & Raj, B. (2008). Magnetic field induced extinction of light in a suspension of Fe<sub>3</sub>O<sub>4</sub> nanoparticles. *Applied Physics Letters*, 92(22), 221911-221913.
- Putra, N., Roetzel, W., & Das, S. (2003). Natural convection of nano-fluids. *Heat and Mass Transfer*, 39(8-9), 775-784. doi: 10.1007/s00231-002-0382-z
- Ranjbar, A. A., Kashani, S., Hosseinizadeh, S. F., & Ghanbarpour, M. (2011). Numerical heat transfer studies of a latent heat storage system containing nano-enhanced phase change material. *Thermal Science*, 15(1), 169-181.
- Salunkhe, P. B., & Shembekar, P. S. (2012). A review on effect of phase change material encapsulation on the thermal performance of a system. *Renewable and Sustainable Energy Reviews*, 16(8), 5603-5616.
- Sato, Y., Deutsch, E., & Simonin, O. (1998). Direct numerical simulations of heat transfer by solid particles suspended in homogeneous isotropic turbulence. *International Journal of Heat and Fluid Flow*, 19(2), 187-192. doi: [http://dx.doi.org/10.1016/S0142-727X\(97\)10023-6](http://dx.doi.org/10.1016/S0142-727X(97)10023-6)
- Trisaksri, V., & Wongwises, S. (2007). Critical review of heat transfer characteristics of nanofluids. *Renewable and Sustainable Energy Reviews*, 11(3), 512-523.
- Velraj, R., Seeniraj, R., Hafner, B., Faber, C., & Schwarzer, K. (1999). Heat transfer enhancement in a latent heat storage system. *Solar energy*, 65(3), 171-180.
- Versteeg, H. H. K., & Malalasekera, W. (2007). *An introduction to computational fluid dynamics: the finite volume method*: Pearson Education Australia.
- Wasp, E. J., Kenny, J. P., & Gandhi, R. L. (1979). *Solid-liquid flow slurry pipeline transportation*: Gulf Pub. Co.
- Wong, K. V., & De Leon, O. (2010). Applications of nanofluids: current and future. *Advances in Mechanical Engineering*, 2010.
- Wu, S., Zhu, D., Li, X., Li, H., & Lei, J. (2009). Thermal energy storage behavior of Al<sub>2</sub>O<sub>3</sub>-H<sub>2</sub>O nanofluids. *Thermochimica Acta*, 483(1-2), 73-77. doi: <http://dx.doi.org/10.1016/j.tca.2008.11.006>
- Xuan, Y., & Li, Q. (2000). Heat transfer enhancement of nanofluids. *International Journal of Heat and Fluid Flow*, 21(1), 58-64.
- Xuan, Y., & Roetzel, W. (2000). Conceptions for heat transfer correlation of nanofluids. *International Journal of Heat and Mass Transfer*, 43(19), 3701-3707.

- Yu, W., France, D. M., Routbort, J. L., & Choi, S. U. (2008). Review and comparison of nanofluid thermal conductivity and heat transfer enhancements. *Heat Transfer Engineering*, 29(5), 432-460.
- Zalba, B., Marín, J. M., Cabeza, L. F., & Mehling, H. (2003). Review on thermal energy storage with phase change: materials, heat transfer analysis and applications. *Applied thermal engineering*, 23(3), 251-283.